Journal Pre-proof

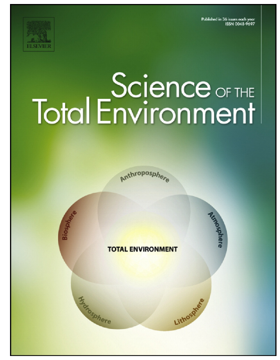

Sources of major elements and nutrients in the water cycle of an undisturbed river basin – Samothraki Island, Greece

Nikolaos Th. Skoulikidis, Ioannis Matiatos, Panagiotis Michalopoulos, Evangelia Smeti, Cemil Özkan, Konstantinos Akepsimaidis, Sofia Laschou, Christine Stumpp

PII: S0048-9697(23)03984-0

DOI: https://doi.org/10.1016/j.scitotenv.2023.165361

Reference: STOTEN 165361

To appear in: *Science of the Total Environment*

Received date: 31 March 2023

Revised date: 19 June 2023

Accepted date: 4 July 2023

Please cite this article as: N.T. Skoulikidis, I. Matiatos, P. Michalopoulos, et al., Sources of major elements and nutrients in the water cycle of an undisturbed river basin – Samothraki Island, Greece, *Science of the Total Environment* (2023), https://doi.org/10.1016/j.scitotenv.2023.165361

Sources of major elements and nutrients in the water cycle of an undisturbed river basin – Samothraki Island, Greece

Nikolaos Th. Skoulikidis[1]*, Ioannis Matiatos[1], Panagiotis Michalopoulos[2], Evangelia Smeti[1], Cemil Özkan[3], Konstantinos Akepsimaidis[1], Sofia Laschou[1], Christine Stumpp[3]

[1]Institute of Marine Biological Resources & Inland Waters, Hellenic Centre for Marine Research (HCMR), 46.7 km Athens-Sounion Ave., 19013 Anavyssos, Attika, GREECE

Institute of Oceanography, Hellenic Centre for Marine Research (HCMR), 46.7 km Athens-Sounion Ave., 19013 Anavyssos, Attika, GREECE

[3]University of Natural Resources and Life Sciences, Vienna, Department of Water, Atmosphere and Environment, Institute of Soil Physics and Rural Water Management, Muthgasse 18, 1190 Vienna, AUSTRIA

*Corresponding author: nskoul@hcmr.gr

Abstract

We studied the origin of elements of an undisturbed stream basin during the dry season as derived by atmospheric inputs and lithological processes. A mass balance model was applied taking into account atmospheric (rain and vapor) inputs and their origin from marine aerosol and dust, as well as the contribution of rock mineral weathering and dissolution of soluble salts. The model results were enhanced using element enrichment factors, element ratios and water stable isotopes. Weathering and dissolution of bedrock and soil minerals contributed the main element portions, besides sodium and sulfate that chiefly derived from wet deposition. Vapor was shown to contribute water to inland waters of the basin. However, rain was the main source of elements compared to vapor, with marine aerosol being the only atmospheric chloride source, contributing also over 60% of atmospheric sodium and magnesium. Silicate derived from mineral weathering (mainly plagioclase and amorphous silica), while soluble salt dissolution contributed the main portions of the rest of major elements. In headwater springs and streams, element concentrations were more affected by atmospheric inputs and silicate mineral weathering was more intense, contrary to lowland waters that were more affected by soluble salt dissolution. Effective self-purification processes were mirrored in low nutrient levels, despite the significant inputs from wet deposition, with rain being more important contributor than vapor for the majority of nutrient species. Relatively high nitrate concentrations in headwaters were attributed to increased mineralization and nitrification, while the downstream nitrate diminishing was due to prevailing denitrification processes. The ultimate goal of this study is to contribute in establishing stream elements' reference conditions using mass balance modeling approaches.

Key words: mass balance, hydrogeochemistry, weathering, water stable isotopes, water cycle, vapor

1. Introduction

The hydrochemical regime of stream water is shaped by a combination of factors and processes, including atmospheric inputs, weathering and dissolution of minerals from soil and bedrock, groundwater inputs, biological processes, and anthropogenic disturbance (Gibbs, 1970; Garrels and Mackenzie 1971; Cleaves et al., 1970; Meybeck 1983).

Atmospheric water deposition has been long recognized as a substantial source of elements to stream water (Conway, 1942; Gorham, 1958), especially in weathering resistant basins with low solute concentrations (Gibbs, 1970; Meybeck, 1983). In montane areas, additionally to rain and snow, fog may contribute considerable amounts of condensed water (De Jong, 2005) to stream basins, laden with major ions and pollutants (Dollard et al., 1983; Collett et al., 2002). Mineral weathering and dissolution imprint the bedrock composition on stream water (Garrels and Mackenzie, 1971). Groundwater inputs enhance stream water solute concentrations especially at the lowlands where surface- ground-water interactions can be intense (Tripathi et al., 2021). In dry regions, readily soluble secondary salts that accumulate in soil pores, enrich stream water with major ions and nutrients as a result of flashing during flood events (Walling and Foster, 1975; McClain et al., 2003). Biological processes add or remove elements from stream water through decomposition or uptake processes (Velbel and Price, 2007). Finally, anthropogenic activities are responsible for the enrichment of stream water in all major elements, either directly or indirectly, i.e. through calcium/magnesium bicarbonate solubility increase as a result of CO_2 rise induced by organic waste decomposition (Skoulikidis, 2018).

To quantitatively relate the hydrochemical composition of running waters to each one of these driving forces, geochemical mass-balance methods in small watersheds are being commonly used (e.g. Garrels and Mackenzie, 1967, 1971; Cleaves et al., 1970; Miller and Drever, 1977; Bricker et al., 1983; Katz et al., 1985; Velbel, 1985, 1992; Taylor and Velbel, 1991; Furman et al., 1998; Freyssinet and Sarah, 2000; Oliva et al., 2004; Price et al., 2012; Viers et al., 2014; Abe et al., 2019) as a standard method (Velbel and Price, 2007).

Watershed geochemical mass balance approaches introduce a system of equations that simulate the steady-state input–output behavior of an aquatic system at a stream basin scale (Bricker et al., 2003). Elemental mass-balances mainly include element inputs by precipitation, mineral weathering, biomass decomposition and desorption from soils, whereas element outputs include clay mineral formation, adsorption on soils and botanical uptake (Viers et al., 2014; Velbel and Price, 2007).

Stable isotopes of water (^{18}O and ^{2}H) provide important information about the source signatures of the water cycle components, including precipitation origin, moisture and vapor sources, and evaporation processes (Clark and Fritz, 1997; Vespasiano et al., 2015; Matiatos and Wassenaar, 2019; Villalobos-Forbes et al., 2021; Vystavna et al., 2021a). Moreover, stable isotope techniques have been widely used to understand the interaction between precipitation (including fog) and the terrestrial water bodies, such as rivers, lakes and groundwater (e.g., Blarasin et al., 2020; Matiatos et al., 2014, Li et al., 2020; Vystavna et al., 2021b) and trace the relative contributions of potential solute sources to surface- and groundwater (Kendal and Caldwell, 1998).

The contribution of geochemical mass balance models in answering fundamental planetary questions, such as soil formation rates, nutrient replenishment for biota (Amundson et al., 2007), and consumption rates of atmospheric CO_2 through silicate chemical weathering related to the Earth's climate (Berner et al., 1983; Dessert et al., 2003), is well known. In addition, mass balance approaches may be proved a useful tool in a basin or water body scale as a basis to back-cast the quality of disturbed surface water systems (Meybeck, 2003), and to assist process-based river basin restoration (Beechie et al., 2010). When reference conditions are lacking, the estimation of natural elemental back ground levels using weathering mass-balance approaches may serve as a measure to assess the deviation of a water body from reference conditions, thus solving fundamental Water Framework Directive (WFD 2000/60/EC)-related constraints. Furthermore, understanding the processes shaping the hydrochemical composition of a water body can provide evidence towards targeted and more effective and economical process-based water bodies restoration. However, it is essential, initially, to understand and determine the rates of these processes under natural conditions, as pollution and physical disturbances brought by human activities alter the natural weathering rates and the natural hydrochemical regime of aquatic systems (Viers et al., 2014) and makes the separation of the different water quality contributors and processes more complicated (Hilberg and Riepler, 2016).

Thus, undisturbed or minimally disturbed aquatic ecosystems may serve as the baseline for disentangling elemental natural background levels. However, the availability of such ecosystems is low, both worldwide and in a European scale (Meybeck, 2003; EEA, 2018), while focusing on Mediterranean Europe, the long history of human presence created a deficiency in reference conditions (Hering et al., 2010). In the frame of this study, we selected the small, monolithological Fonias basin on Samothraki Island, NE Aegean Sea, one of the last minimally disturbed islands in the Mediterranean (Skoulikidis et al., 2014; Skoulikidis et al.,

2020) and applied a set of methods to quantify surface- and groundwater element sources as derived from the different components of the water cycle during the dry period of the year.

To the authors knowledge, innovations of this study include the addition of vapor as wet deposition contributor to mass-balance models, and the validation of the mass-balance approach using water stable isotopes, among other independent methods. The novel idea of using mass balance modeling in establishing elements' reference conditions in stream ecosystems may affect future mass balance model applications.

2. Methodology

2.1. Study area

A detailed description of the physical and anthropogenic characteristics of Samothraki Island is presented in Skoulikidis et al. (2020). The Fonias basin (9.5 km^2) (Fig. 1) is mountainous (mean basin altitude 795 m asl) and steep (mean basin slope 21.9°) and is composed almost exclusively by a highly deformed and eroded porphyritic quartz monzonite to granite pluton (Christofides et al., 2000; Panagopoulos et al., 2019) with limited regolith cover (Skoulikidis et al., 2020) (Fig. S1-supplementary material), as a result of still ongoing uplift tectonic movements (Syrides et al., 2009). The stream has a total length of 37.4 km, is perennially flowing (average annual discharge 0.48 m^3/s), has a stream order after Strahler of 4 and a flashy flow regime (specific discharge 27.5 L/s×km). Numerous small springs connected with shallow, fractured aquifers of low capacity and small brooks contribute to the streams' hydrograph, developing a dendritic pattern with relatively high drainage density (3.9 km/km^2). The basin is uninhabited and uncultivated, and anthropogenic disturbance comprise the reduction of woodland cover through the past two centuries (Heiling, 2018) in combination with more recently introduced intense free grazing livestock (Noll et al., 2020). Apart of a riparian plane forest that borders the stream along its entire course, the vegetation cover in the watershed is poor and mainly consists of shrub, while bare rock surfaces dominate; natural grasslands, sclerophyllous vegetation, transitional woodland-shrub areas and bare rock surfaces occupy 94.4 % of the basin, broad-leaved forests cover 4.1 % and land principally occupied by agriculture with significant areas of natural vegetation 1.5 % (EEA, 2020).

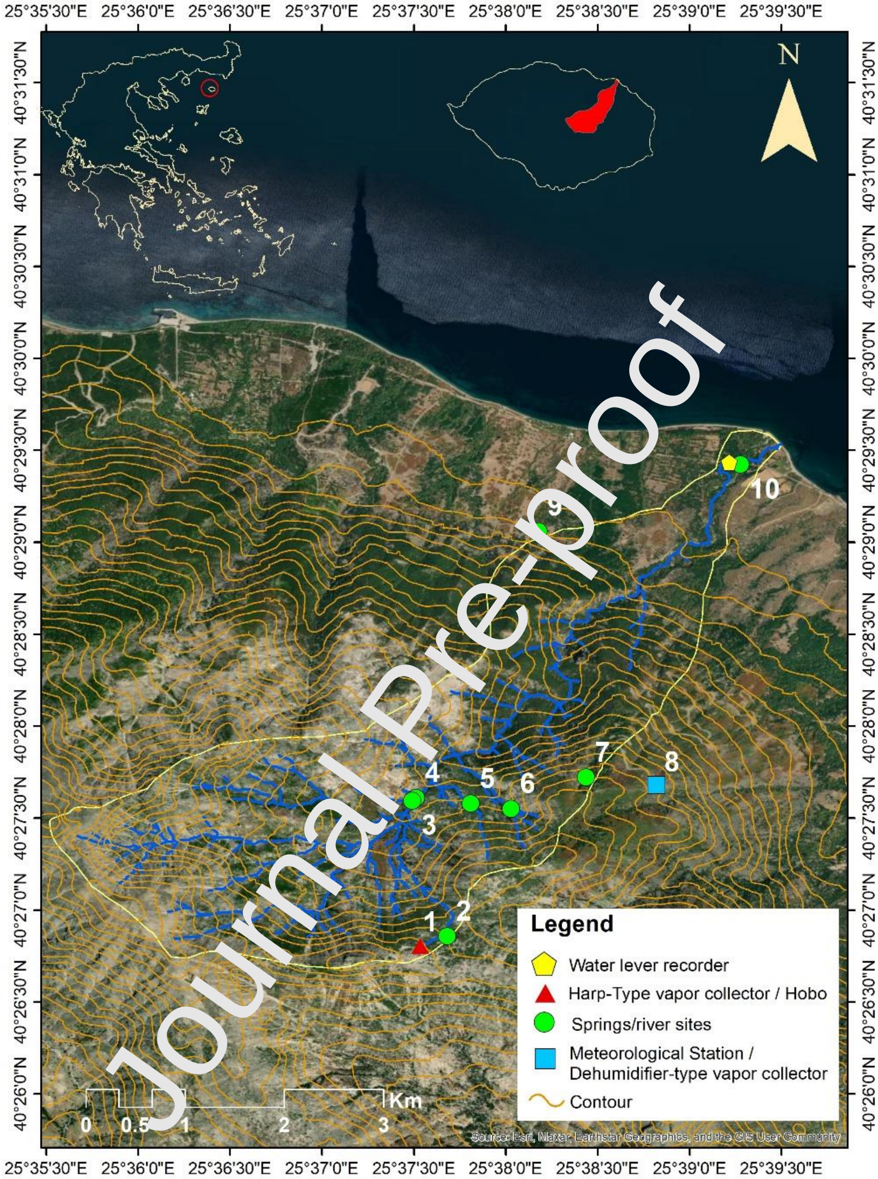

Figure 1. The Fonias basin with contours, the hydrographic network, the monitoring stations and the sampling sites. 1: harp-type vapor collector and Hobo, 2: Amoni (Am) spring; 3: Fonias upstream (F-us), 4: Itamos (It) spring, 5: 2nd Fonias tributary (2nd T), 6: 1st Fonias tributary (1st T), 7: Barrels (Ba) spring, 8: meteorological station and dehumidifier-type vapor collector, 9: Ag. Antonios (AA) spring, and 10: water level recorder and Fonias downstream (F-ds).

2.2. Methods

2.2.1. Data collection

Meteorological, hydrological, and hydrochemical data were collected from July to September 2021 (10/7 to 26/9/2021). Meteorological data were collected by an automatic, telemetric meteorological station (ExMachina, Froggit WH3000 SE PRO; time-step 60 min) at an altitude of 780 m asl, operated by the Hellenic Centre for Marine Research (HCMR). At the beginning of July, an automatic Hobo instrument (time-step 30 min) was installed close to the meteorological station for five days to compare air temperature and relative humidity between the two instruments. Hydrological data were gathered using an automatic telemetric ultrasonic water level recorder (ExMachina, Maxbotix MB7076 XL, time step 60 min) mounted near the stream outflow (Fig.1).

In total, 17 event-based rain (R) water samples were collected within or close to Fonias river basin using bulk rain collectors targeting water stable isotope analysis. Two of them were placed to collect long-term rain (LTR) samples. In particular, 7 of the rain events were collected during the field work period (July-September 2021), whereas the rest were collected by volunteers prior to the actual field work (May – beginning of July). All rain samples were gathered immediately after the events and stored in a refrigerator. Vapor (V) samplings were carried out using a power supplied dehumidifier, as active fog collector, and a passive harp-type wire fog collector (Fischer and Still, 2007). The active fog collector was installed close to the meteorological station (at 780 m asl), and was equipped with a hygrostat to collect vapor by air humidity > 85 %. By these means, 11 vapor samples were collected directly after fog events and three additional long-term vapor samples (LTV). To avoid evaporation, vapor that accumulated during night and early day hours was collected early in the morning, before the fog cleared, and stored within an hour in the refrigerator. The passive fog collector was installed at an altitude of 1095 m asl. To avoid evaporation, vapor from the collector was gathered in a 500 ml High Density Polyethylene (HDPE) vial placed at 0.5 m underground.

Due to the difficulty to access this station, only one composite (vapor plus rain) long-term sample (named long-term vapor/rain sample; LTV/R) was possible to be collected several days after the events.

Hydrochemical data were obtained from rain, vapor, stream, and spring samples. In-situ measurements and samplings were performed at Fonias upstream and downstream (F-us and F-ds), two Fonias stream tributaries, called first and second tributary (1^{st} T, 2^{nd} T), and four springs; three upstream ones, i.e. Amoni (Am), Itamos (It) and Barrels (Ba) and a lowland spring (Ag. Antonios; AA) (Fig. 1). Hourly samplings during and after a rain event on 22 September were additionally performed at the Ba spring, the 1^{st} T, 2^{nd} T and at F-ds. In total, 21 spring samples and 32 stream samples were collected. Finally, regarding water stable isotopes, four additional post-rain samples were collected by volunteers at F-ds in May.

For major ions and nutrients, rain, spring, and stream samples were collected in 500 ml HDPE bottles, preserved using 0.5 ml $HgCl_2$ and stored in the refrigerator. For chloride analysis, extra samples were collected in 50 ml plastic vials and stored in the refrigerator.

2.2.2. Field measurements and laboratory analysis

Physicochemical measurements (water temperature, electrical conductivity, dissolved oxygen and pH) in springs and streams and, where possible (according to the collected volume of water), in rain and vapor were carried out in-situ using a HANNA 98194 portable device.

Water samples were analyzed for water stable isotopes at the University of Natural Resources and Life Sciences, Vienna (Austria) and for major ions (Ca^{2+}, Mg^{2+}, Na^+, K^+, HCO_3^-, CO_3^{2-}, Cl^-, SO_4^{2-}), Si, water hardness and nutrients [NO_3^-, NO_2^-, NH_4^+, PO_4^{3-}, total nitrogen (TN) and total phosphorous (TP)], at the HCMR laboratory after being filtered with 0.45 μm pore size membrane filters.

Major ions were measured by ion chromatography using a 940 Professional Metrohm Ion Chromatographer. Hydrogen carbonate and carbonate were determined by titration with 0.1 N

HCl and the proper selective electrode using a Metrohm Omnis automatic titrator. The limits of quantitation (LOQs) were: 0.74 mg/l for Ca^{2+}, 0.43 mg/l for Mg^{2+}, 0.27 mg/l for Na^{+}, 0.46 mg/l for K^{+} and 0.17 for Cl^{-} . Nitrate, nitrite, ammonium, orthophosphate and silicate were determined by a Skalar San++ Continuous Flow Analyzer according to standard methods (for ammonium Kerouel and Aminot, 1997; for phosphate Boltz and Mellon, 1948; for nitrate and nitrite Navone, 1964; for silicate Babulak and Gildenberg, 1973. The limits of quantitation (LOQs) were: 1 μg/l for nitrite ($N\text{-}NO_2^-$), 2 μg/l for nitrate ($N\text{-}NO_3^-$), 1 μg/l for phosphate ($P\text{-}PO_4^{3-}$), 5 μg/l for ammonium ($N\text{-}NH_4^+$) and 0.20 mg/l for silicate. The determination of total Nitrogen (TN) and total Phosphorus (TP) was performed by the wet chemical oxidation method, WCO, according to Raimbault et al. (1999). According to this method, after oxidation/digestion all nitrogen and phosphorus organic compounds convert respectively to inorganic salts. The assay mixture was analyzed for nitrates and phosphates. The analysis was performed with a Skalar Auto analyser as mentioned above. Organic nitrogen (ON) and organic phosphorous (OP) were obtained from the differences between total dissolved nitrogen (TN) and dissolved inorganic nitrogen (DIN = $N\text{-}NO_3^-$ + $N\text{-}NO_2^-$ + $N\text{-}NH_4^+$) and between total P (TP) and P- PO_4^{3-}, respectively. Finally, Total Dissolved Solids (TDS) of each water sample was calculated by adding major ions and silica concentrations.

Water stable isotope ratios ($^{18}O/^{16}O$ and $^{2}H/^{1}H$) were analyzed using a Picarro L2140-i series. The isotope values were expressed in delta (δ) units with a per mil (‰) notation relative to Vienna Standard Mean Ocean Water (VSMOW):

$$\delta_{\text{sample}}\ (‰) = \left(\frac{R_{sample}}{R_{VSMOW}} - 1\right) \times 1000$$

where R_{sample} and R_{VSMOW} is the $^{18}O/^{16}O$ or $^{2}H/^{1}H$ ratio of the sample and the standard for $\delta^{18}O$ and $\delta^{2}H$, respectively. The analytical uncertainty was ±0.1 ‰ for $\delta^{18}O$ and ±0.5 ‰ for $\delta^{2}H$.

Gaps in measurements were due to the following facts: rainfall samples collected by volunteers prior the actual field work targeted only water stable isotopes; the collected volume of a number of vapor and rainfall samples during the field work samplings was insufficient to perform all chemical analyses; and a defect of the portable device did not allow us to measure physicochemical parameters during the last day of field work.

2.2.3. Data analysis

2.2.3.1. Hydro-meteorological data

Hourly meteorological data, including air temperature (AT), relative humidity (RH), solar radiation (SR), rainfall (P), wind speed (WS), and direction (WD) were analyzed. To assess relationships between RH and other meteorological data, we calculated mean values of the other meteorological parameters for RH≥85 % and RH<85 %. To compare increased RH with fog events, field observations were supplemented with satellite images (NASA, 2022). To distinguish any day-night meteorological differences, we calculated average meteorological parameters for SR=0 (night) and SR>0 (day). The number of night hours was 9-11, according to the month. To assess the average meteorological data at different wind directions, eight wind direction classes were used, i.e. N-NE (0-44^o), NE-E (45-89^o), E-SE (90-134^o), SE-S (135-179^o), S-SW (180-224^o), SW-W (225-<269^o), W-NW (270-<314^o) and NW-W (315-360^o). Finally, to estimate the impact of wind speed on the other meteorological parameters, we classified wind speed into 4 categories: 0-3, >3-6, >6-9, and >9 m/s and calculated average values for each one. Finally, water level data were analyzed to assess daily and hourly fluctuations and day-night differences. To convert water level to discharge, an existing stage-discharge rating curve were applied (Skoulikidis et al., 2020).

2.2.3.2. Hydrochemical data

A Piper diagram was used to demonstrate the hydrochemical variability of the stream and spring samples under investigation, using Geochemist Workbench. To assess the relationships between major ions, silica, and nutrients in atmospheric and inland waters, Spearman rank correlations were carried out for stream and spring samples separately. To assess the relationships among the different components of the water cycle, i.e. rain, vapor and the inland waters' (surface and groundwaters) sampling sites, two cluster analyses on normalized data, using Euclidean distance and group average, were carried; one on major cations, sulfate and silica, and one on nutrients, i.e. nitrate, nitrite, ammonium, phosphate, TP, organic nitrogen (ON) and organic phosphorus (OP). Hydrogen carbonate and chloride were excluded since a number of atmospheric samples was incompletely analyzed due to inadequate volume of water collected. Finally, a simper analysis was performed for the groups produced by the cluster analysis. Spearman rank correlations were performed in R programming language (v. 4.0.3; R Core Team, 2020), package Hmisc v.4.7-2 (Harrel, 2022). Cluster and simper analyses were performed in Primer 6 (Clark and Gorley, 2006). Since in the majority of atmospheric samples a portion of elements were below LOQ, for multivariate analysis the $\frac{\mathrm{LOQ}}{2}$ values were applied (Antweiler et al., 2015).

To assess stream nutrient quality for each site, the median values of nutrient species were compared to the nutrient thresholds according to the Hellenic Nutrient Quality Index (HWQI) (Skoulikidis et al., 2006; Panagopoulos et al., 2022). For comparison reasons, the system was also applied to atmospheric samples and springs.

As a first approach to apportion the marine influence on the elements of surface and ground waters, we calculated their enrichment factors (EF), by comparing their ratios in the examined waters to the sea water ratios (Wu et al., 2008; Wang et al., 2019; Keresztesi et al., 2019), according to the equation:

$$\mathrm{EF\ seawater} = \frac{\frac{\mathrm{X}}{\mathrm{Cl}}\ \mathrm{freshwater}}{\frac{\mathrm{X}}{\mathrm{Cl}}\ \mathrm{seawater}}$$

where X is the concentration of the ion of interest, $\frac{\mathrm{X}}{\mathrm{Cl}}$ freshwater represents the ratio of X ion to chloride found in the examined waters, whilst $\frac{\mathrm{X}}{\mathrm{Cl}}$ seawater is the respective ratio in seawater. An ion is considered to show high affinity to sea water when the EF is close to the unit, and it is enriched relatively to seawater if the EF value is higher than the unit.

We used chloride as reference element, since sodium in the basin and the broader area derives additionally from silicate weathering, and it is thus expected to be contained in atmospheric dust. This is confirmed by the average Na/Cl molar ratio of the stream basin waters (1.15), which exceeds the respective seawater ratio (0.86). Assuming that chloride originates only from marine sources, this element may be used as the basis to approximately detect seawater contribution for other elements found in atmospheric sources and inland waters (Meybeck, 1983; Rao et al., 2016).

Considering the fact that a hydrological-, and thus an elemental-, flux balance approach (Cleaves et al., 1970) is not realistic to be applied for only a portion of the hydrological year (dry period), to quantify the lithologic sources of elements in the stream basin, a simple elemental mass-balance model has been applied:

To estimate the atmospheric contribution of major ions and silica (from now on termed elements) to inland waters (surface- and groundwaters), the mean molar element concentrations of wet deposition (rain plus vapor) were subtracted from the respective concentrations measured in inland waters (Garrels and Mckenzie, 1971; Meybeck, 1996; Wu et al., 2008, Harmon et al., 2013). This approach was applied for each element and sampling site separately. Due to insufficient sample volume, chloride was not measured in rain, and bicarbonate neither in rain nor in vapor samples. Thus, chloride data were taken from literature (Skoulikidis et al., 2020). Regarding bicarbonate, we assumed that the minimum concentration found in the basin was entirely due to wet deposition (rain and vapor) (Wu et al., 2008; Li et al., 2019). The same procedure has been applied for calcium, magnesium and potassium, as their concentrations in rain and vapor exceeded their minimum concentrations in the basin waters.

Furthermore, we assumed that the ionic ratios of marine aerosol resemble to those of sea water, and that all chloride in wet deposition (rain plus vapor) derives from marine aerosol. Then, based on the chloride concentration in wet deposition and the elemental sea water composition we calculated stoichiometrically the respective molar concentrations of elements that can be assigned to marine aerosol. The results of this approach were compared with the EF approach using linear correlations for each element separately.

By subtracting the elemental molar concentrations of marine aerosol from the total concentrations in wet deposition (rain plus vapor), we estimated the concentration and portion of elements that derive from other atmospheric sources (i.e., dust particles and/or atmospheric pollution).

Considering only minimal anthropogenic terrestrial sources (i.e., small free grazing ruminants; Skoulikidis et al., 2020), and assuming that biological processes in the basin are in steady-state (Drever and Clow, 1995; Likens and Boorman, 1994; Viers et al., 2005; Abe et al., 2019), we estimated the concentration and portion of elements released from lithological sources by subtracting the atmospheric (rain plus vapor) concentration from the mean stream or spring concentration for each element and for each sampling site separately.

We finally applied the elemental mass-balance model, first introduced by Garrels and Mckenzie (1967) to allocate the purely geogenic element portion of inland waters to particular mineral weathering and salt dissolution reactions. To assess the type of the clay mineral formed through rock mineral weathering we applied mineral stability diagrams (log SiO_2 vs log K^+/H^+ and log K^+/H^+ vs log Mg^{2+}/H^+) with the Geochemist's Workbench (https://www.gwb.com/).

The relative portions of orthoclase, plagioclase, hornblende, and biotite in the granite of Fonias basin were estimated as follows: The sum of hornblende plus biotite on the basis of their average Ti, Fe, Mn and Mg portions, compared to the portions measured in the Fonias basin bedrock, according to Christofides et al. (2000). We then assumed a biotite to amphibole ratio of 1.33, according to the estimations of Seymour et al. (1996). The granite is termed porphyritic quartz monzonite (Christofides et al., 2020). It thus includes a relatively high portion of plagioclase (30-65 %). Based on the estimations of Seymour et al. (1996), we assumed an orthoclase to plagioclase ratio of 1.07. Thus, the granite composition used (excluding quartz) was: 48.6 % orthoclase, 45.5 % plagioclase, 3.4 % biotite and 2.5 % hornblende, by weight. The formulas of plagioclase, biotite and hornblende have been estimated using the elements' oxides of these minerals in quartz monzonite (Christofides et al., 2000), according to the methods of Leake et al. (1997) and Brady et al. (2022), assuming iron in biotite and hornblende is in the form of Fe^{+2} and aluminum is conserved between initial reactant phases (biotite, hornblende, plagioclase, orthoclase) and kaolinite as the final product during weathering. The applied sequence of silicate mineral reactions followed the Goldichs's order of weatherability (Goldich, 1938) from less to more weathering resistant minerals, i.e. biotite, hornblende, plagioclase and orthoclase.

Using the portion of biotite in Samothraki granite we assigned 3.4 % of silica found in the precipitation-corrected spring and stream water sites, together with stoichiometric amounts of potassium, magnesium and bicarbonate (in mmol/l) to the weathering of biotite to kaolinite, according to the following reaction:

$$K_{0.9}(Mg_{1.43}Fe^{2+}_{1.14}Mn_{0.04}\,Ti_{0.26})(Al_{1.2}\,Si_{2.8})O_{10}(OH)_2 + 8.34\,CO_2 + 1.44\,O_2 + 8.14\,H_2O = 0.9\,K^+ + 1.43\,Mg^{2+} + 1.14\,FeOOH + 0.26\,TiO_2 + 0.04\,MnO_2 + 1.6\,H_4SiO_4 + 8.34\,HCO_3^- + 0.6\,Al_2Si_2O_5(OH)_4$$

We then assigned 2.5 % of silica, together with stoichiometric amounts of sodium, calcium, magnesium and bicarbonate to hornblende weathering according to the reaction:

$$(Ca_{1.8}\,Na_{0.42})(Mg_{3.06}Fe^{2+}_{1.83}Al_{0.27})(Al_{0.81}Si_{7.19})O_{22}(OH)_2 + 15.83\,CO_2 + 1.83\,O_2 + 21.13\,H_2O = 0.42\,Na^+ + 1.8\,Ca^{2+} + 3.06\,Mg^{2+} + 1.83\,FeOOH + 6.11\,H_4SiO_4 + 15.83\,HCO_3^- + 0.54\,Al_2Si_2O_5(OH)_4$$

Similarly, we allocated 45.5 % of silica and related elements to plagioclase weathering, according to the reaction:

$$Na_{0.65}Ca_{0.34}Al_{1.36}Si_{2.65}O_8 + 1.32\,CO_2 + 4.6\,H_2O = 0.64\,Na^+ + 0.34\,Ca^{2+} + 1.29\,H_4SiO_4 + 1.32\,HCO_3^- + 0.68\,Al_2Si_2O_5(OH)_4$$

We then assigned 10% of the remaining potassium to orthoclase weathering, according to the following reaction:

$$KAlSi_3O_8 + CO_2 + 5.5\ H_2O = K^+ + 2\ H_4SiO_4 + HCO_3^- + 0.5\ Al_2Si_2O_5(OH)_4$$

Any elements remaining after silicate weathering reactions were attributed to the dissolution of soluble salts, that may derive from fluid inclusions in minerals (Garrels and Mckenzie, 1971; Drever, 1997; Clow and Sueker, 2000) or accumulate in soil pores or rock fractures during the dry season (e.g., Schofield et al., 2001), in descending solubility order, i.e. calcium chloride, halite, potassium chloride, epsomite, gypsum, calcite and dolomite (HCP, 2022). In order to check the ability of the mineral phases and soluble salts to dissolve, the saturation indices were calculated based on the chemical analysis and physicochemical measurements using PhreeQc. In the case of aluminosilicate minerals this was not feasible due to the lack of dissolved Al data.

2.2.3.3. Isotopic data

The "deuterium excess" or "*d*-excess" was calculated as follows (Dansgaard, 1964):

$$d\text{-excess}\ (‰) = \delta^2H - 8\times\delta^{18}O$$

Mixing model: To investigate the contribution of precipitation in the Ba spring, the tributaries and the F-ds site prior and after the occurrence of the rain event of the 22nd of September (i.e., beginning of rainy period) a two-end member mixing model was applied using the mass balance equations below:

$$f_1(\delta^{18}O_R) + f_2(\delta^{18}O_{XPrior}) = \delta^{18}O_{XPostr}\ \text{(Eq. 1)}$$

$$f_3(\delta^2H_R) + f_4(\delta^2H_{XPrior}) = \delta^2H_{XPostr}\ \text{(Eq. 2)}$$

where R is the rain samples during the 22nd of September with f_1 and f_3 representing their proportional contribution in %, X_{Prior} and X_{Postr} are the samples in Ba springs, tributaries and F-ds prior and after the rain event, respectively, with f_2 and f_4 representing their proportional contribution in % prior the rain event. The average proportional contributions for rain and X_{Prior}

were derived from $(f_1 + f_3)/2$ and $(f_2 + f_4)/2$, respectively, with $f_1 + f_2 = 1$ and $f_3 + f_4 = 1$. No fractionation effect was considered given that the sampling was done immediately after the rain event.

Origin of vapor: To investigate the origin of the vapor samples we calculated the theoretical isotopic composition of vapor ($\delta^{18}O_v$) produced by the local stream waters or the sea ($\delta^{18}O_l$) after considering a total fractionation between the water column and the open air as the sum of fractionation factor for equilibrium water-vapor exchange ($\varepsilon_{l\text{-}v}$) and the kinetic factor ($\Delta\varepsilon_{bl\text{-}v}$) using the following equation (Clark and Fritz, 1997):

$$\delta^{18}O_l - \delta^{18}O_v = \varepsilon_{l\text{-}v} + \Delta\varepsilon_{bl\text{-}v} \quad \text{(Eq. 3)}$$

where $\varepsilon_{l\text{-}v}$ = 9.7 ‰ after assuming an air temperature of 20 °C in the equations of Kakiuchi and Matsuo (1979), and $\Delta\varepsilon_{bl\text{-}v}$ = 2.1 ‰ after assuming a humidity of 85 % in the equations of Gonfiantini (1986). The theoretical isotopic composition of the vapor ($\delta^{18}O_v$) from stream water and sea water was compared with the observed isotopic composition of the vapor.

3. Results

3.1. Hydrometeorological conditions

3.1.1. Meteorological characteristics

During the time of the study, the average values of AT, RH and WS at 780 m asl (Fig. 1, site 8) were 20.9 °C, 60.0 % and 5.7 m/s, respectively. The sum of precipitation (P) was 15.1 mm. At the same time, the sum of P at the meteorological station in Chora of Samothraki (50 m asl) was 13.7 mm. Around 15 % of all measurements revealed RH values ≥85 % (average 92.3 %). According to field observations and satellite images, 14 days within July and August, were marked by fog events; thick layers of fog covered the mountain summits down to about 400 m asl during the night/morning hours until about 12:00 noon. In the night, the average RH was 64.2 %, with 20.3 % of the values exceeding 85 %. During day time, the average RH was 57.1 %, with 14.4 % of the measurements exceeding 85 %. The frequency of measurements with

RH ≥85 % was maximum in September (41.5 %), followed by July (25.1 %) and August (18.9 %). Finally, W-NW and W-SW winds prevailed with frequencies of 39.8 % and 17.8 %, respectively) followed by E-SE and E-NE ones.

To validate the Hobo measurements, a comparison of AT and RH data of the meteorological station and the Hobo for 108 measurements showed satisfactory correlations (r=0.90, at p<0.01, for both variables). The average difference between the meteorological station and the Hobo was +0.6 ^{o}C for AT and -1.6 % for RH.

The comparison of the AT and RH at 780 m asl (meteorological station) and 1095 m asl (Hobo) showed that the average RH and AT at 780 m (20.5 ^{o}C and 60.0 %, respectively) differed insignificantly from that at 1095 m asl (19.3 ^{o}C and 62.3 %, respectively). At both elevations, RH was higher during the night than during the day; the average night RH was 60.1 % and 60.2 % and the average day RH was 54.5 % and 58.4 %, at 780 and 1095 m asl, respectively.

Compared to the other wind direction classes, the prevailing W-NW winds revealed minimum average AT (19.3 ^{o}C), while average RH and wind speed were at the maximum (65.9 % and 8.1 m/s, respectively). During the night, when W-NW winds were blowing, the air temperature dropped to 15.4 ^{o}C, the RH increased to 78.7 % and the wind speed reached 9 m/s. W-SW winds were associated with the second lowest air temperature (20.3 ^{o}C) and the second highest RH and wind speed (61.9 % and 6.5 m/s, respectively). W-SW winds were related with maximum precipitation, which occurred at wind speeds <9 m/s. When W-SW winds were blowing, the night temperature dropped to 16.9 ^{o}C and the RH increased to 73.1 %. W-NW and W-SW winds predominated primarily in July (38 %) and September (35 %) and were less common in August (27 %).

3.1.2. Hydrological characteristics

Fig. 2 illustrates the daily average water level fluctuation during the time of the study, as well as the hourly post-rain water level variation on 22-23/9. During the observation period, the average water level at F-ds was 23.3 cm. No significant difference in monthly water levels was observed (Fig. 2) as evidenced by the average and median values and the low coefficient of variation. Excluding the days with rain events (30/8 and 22/9), a 13 % increase of water level (average 2.9 cm or 0.07 m^3/s) during the night (20:00'- 7:00') was detected compared to the day (7:30'- 19:30'). This trend was evident every day.

The light rain events during August only slightly affected water level at F-ds. On the contrary, the rain event of 22/9 (6 mm in late afternoon-22:00') triggered a water level rise, starting 2 hours after the end of the rain event (22/9 at 24:00'), reaching its peak (33 cm) after 5 hours (23/9 at 5:00') and ending 11 hours after the end of the rain event (23/9 at 21:00') (Fig. 2).

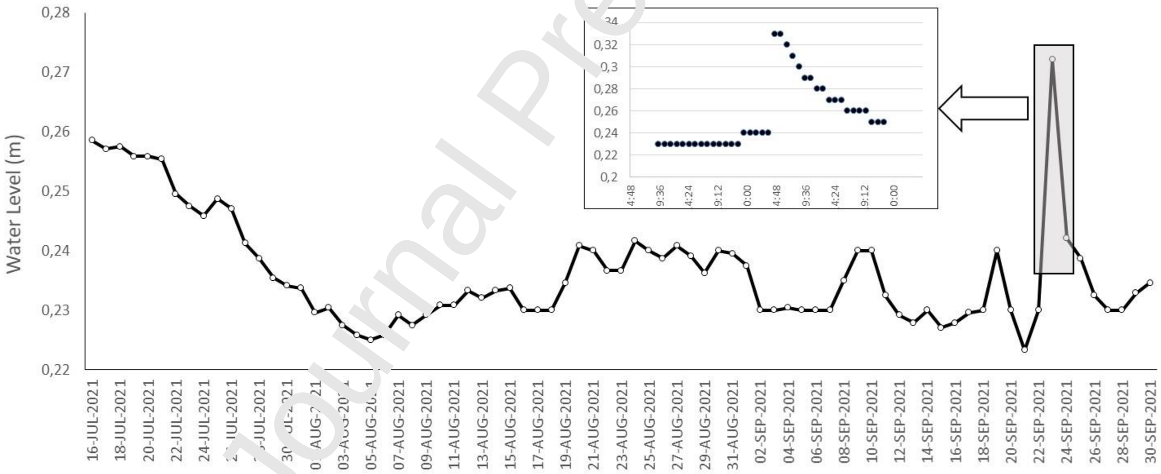

Figure 2. Daily water level fluctuation (in m) during the time of investigations at the F-ds gauging station (time step 60') and a snapshot of post-rain (22-23/9) hourly water level variation.

3.2. Hydrogeochemical characteristics

3.2.1. Element distribution in the water cycle components

3.2.1.1. Major ions and silica

Regarding spring and stream samples, the total cation – total anion Spearman correlation coefficient (*r*) was 0.95 (*p*<0.01), and the median and absolute median $\frac{TK-TA}{TK+TA} X\,100$ were -2.14 and 3.1, respectively.

Fig. S2 illustrates the hydrochemical variability of the examined stream and spring samples. The most common hydrochemical type (using meq/l) was calcium bicarbonate (Ca^{2+}>Na^{+}>Mg^{2+}>K^{+} - HCO_3^{-}>Cl^{-}>SO_4^{2-}), representing ¾ of spring and ¾ of stream samples (AA, Ba, two out of four Am samples, two out of three F-us samples, four out of five 1st T samples, and F-ds). The rest of the samples fitted to a sodium type; the sodium bicarbonate type (Na^{+}>Ca^{2+}>Mg^{2+}>K^{+} - HCO_3^{-}>Cl^{-}>SO_4^{2-}) predominated and was represented by the 2nd T and the early summer samples of the F-us, the 1st T and two Am spring samples. Finally, the It spring fitted in a sodium chloride type (Na^{+}>Ca^{2+}>Mg^{2+}>K^{+} - Cl^{-}>HCO_3^{-}>SO_4^{2-}).

Two of the three rain samples (where only cations and sulfate were determined) were of a sodium-type and one of a calcium-type. In most of the vapor and the long-term vapor (LTV) samples, major ions and silica fell under the LOQ. The long-term rain (LTR) sample was of a calcium bicarbonate type, while the long-term vapor/rain (LTV/R) sample was of a sodium chloride type.

The average TDS of springs was 92.1 mg/l, with AA spring showing the highest value (181 mg/l). On the contrary, headwater springs revealed minimum TDS (It 38.2 and Am 46.4 mg/l), compared to all inland waters examined, followed by Fonias upstream (F-us) (51.9 mg/l) and the two tributaries (average 53.2 mg/l). The LTV/R sample showed maximum mineralization (TDS 532 mg/l), followed by the LTR sample (144 mg/l) (Fig. 3a, Table S1a).

In general, major ion concentrations in LTR and LTV/R, exceeded the inland water levels (Fig. 3a, Table S1a). On the contrary, rain (R), vapor (V) and LTV samples were less enriched than inland waters regarding major ions, besides potassium and sulfate that revealed higher concentrations in rain (R) compared to a number of inland waters (Fig. 3a, Table S1a). All atmospheric samples were particularly poor in silica. On average, springs were more enriched in magnesium, silica, sodium, chloride and bicarbonate compared to surface waters. However, headwater springs such as It and Am revealed exceptionally low concentrations in all ions and the Ba spring was poor in chloride, sodium, sulfate and potassium. In contrast, the downstream AA spring was highly mineralized, especially regarding calcium and bicarbonate. All springs were particularly rich in silica. Finally, compared to the springs' average, the main course of Fonias was more enriched in sulfate and the F-ds was more enriched in calcium and potassium.

Directly after the rain event, only hydrogen carbonate revealed a clear decreasing trend in F-ds and the Ba spring (Fig. 3a, Table S1a), whereas in the two tributaries a post-rain TDS increase was observed. Potassium concentration was particularly enhanced in post-rain samples of the two tributaries.

In line with the silicate nature of the stream basin, pH in the stream and the tributaries was low (average 6.51), with maximum value at F-ds (6.83). The tributaries showed particularly lower pH levels (average 5.75). In spring waters, the pH ranged from 5.07 (It) to 6.67 (AA). Among the atmospheric samples, the LTV/R sample showed the lowest pH value (5.88), followed by the vapor (6.53), the LTV (6.55) and the LTR (6.63) samples (Table S1b). Dissolved oxygen concentration was high, both in streams and springs (average 9.7 and 10.4 mg/l, respectively).

Regarding streams, calcium, magnesium, sodium and bicarbonate where highly correlated with each other (r: 0.89-0.95, p<0.001). The aforementioned cations correlated less with chloride and sulfate (r: 0.66 and 0.88, respectively, p<0.001). Potassium was correlated with sulfate, especially when including post-rain samples (r: 0.81, p<0.001), and less with the other cations and anions (r: 0.54-0.77, p<0.001). Its correlation with potassium was far more significant than with silicate. Finally, chloride showed best correlations with sodium and magnesium (r: 0.80 and 0.78, respectively, p<0.001), whereas silica presented relatively week correlations with ions.

In spring waters, cations, bicarbonate and chloride showed high correlations with each other (r: 0.79 - 0.96, p: <0.005 - <0.001). Sulfate revealed weak correlations with other major ions, and only its correlation with sodium was satisfactory (*r*: 0.61, *p*:0.02). When excluding It spring from the analysis, the correlations among sulfate and the other ions improved substantially (*r*: 0.70-0.93, *p*<0.01 - <0.001). Finally, silica did not correlate significantly with any ion.

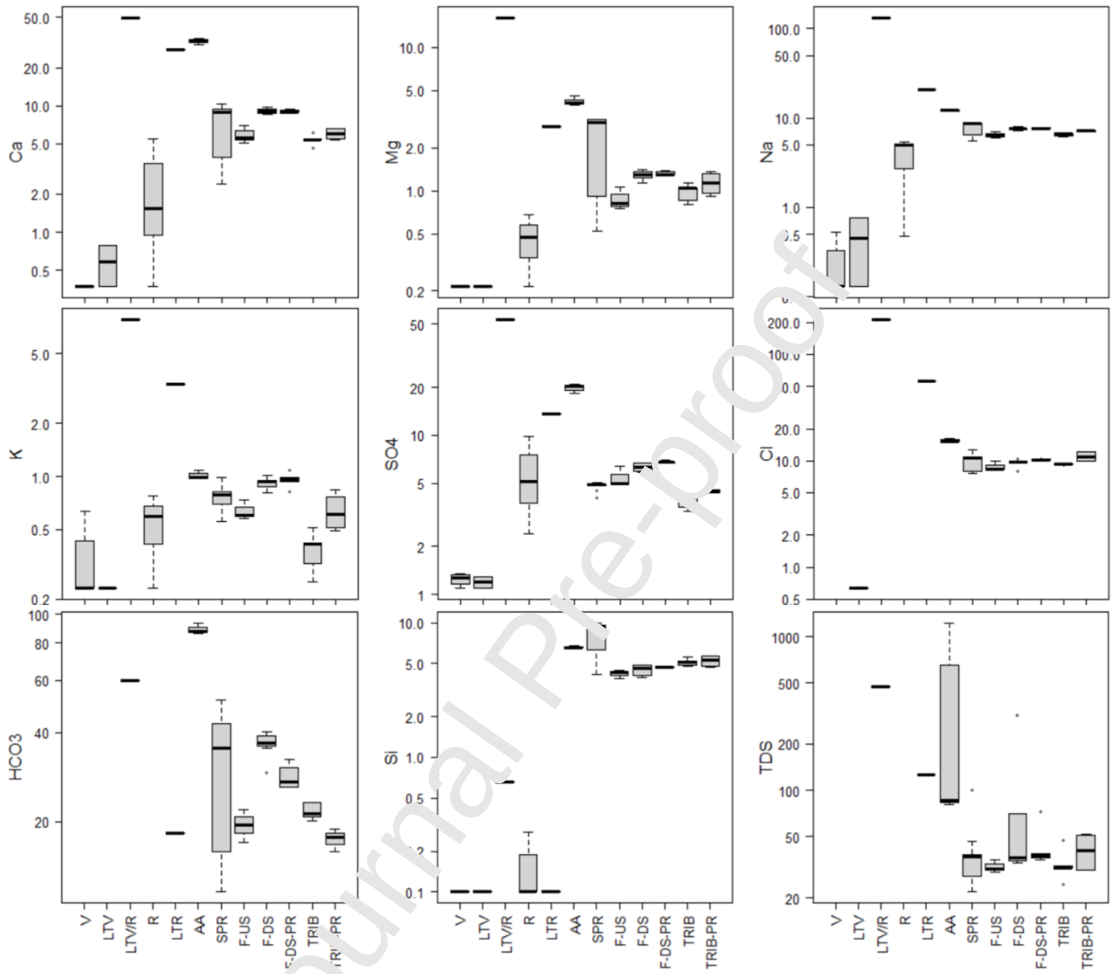

Figure 3a. Box plots of major ions, silica and TDS (mg/l) in the different aquatic systems examined. V: vapor samples, LTV: long-term vapor sample, LTV/R: long term vapor and rain sample, R: rain samples, LTR: long-term rain sample, AA: Agios Antonios spring samples, SPR: spring samples except AA, F-US: Fonias upstream, F-DS: Fonias downstream, F-DS-PR: Fonias downstream post rain, TRIB: tributaries, TRIB-PR: tributaries post-rain. Y-axis is in log scale. The AA spring was kept separately since it differed hydrogeologically from the other springs.

3.2.1.2 N-P nutrients

In the LTV/R and LTR samples, nutrient concentrations exceeded by orders of magnitude stream and spring water levels. The LTV sample also exceeded nutrient levels in streams and springs (especially regarding ammonium and nitrite), apart from nitrate (Fig. 3b, Table S1b). Vapor (V) exceeded the rain levels regarding phosphate, nitrite and OP, whereas rain exceeded vapor concentrations regarding nitrate, ammonium and ON (Table 1). Compared to the average of spring and stream waters, vapor revealed substantial phosphate, ammonium and nitrite enrichment, whereas nitrate was more enriched in inland waters. Compared to the average of spring and stream waters, rain was enriched in all nutrient species, and particularly regarding ammonium (Table 1). Finally, regarding ON% and OP% (organic N and P portions relatively to TN and TP, respectively), atmospheric and inland water samples illustrated comparable levels, besides the LTV/R sample which exhibited minimum levels (Fig. 3b, Table S1b).

Table 1. Nutrient species concentration ratios between average vapor (V, *n*=4), rain (R, *n*=6) and inland waters (IW, *n*=44). Long-term atmospheric samples are excluded. Inland waters: springs and streams

	$N\text{-}NO_3^-$	$N\text{-}NO_2^-$	$N\text{-}NH_4^+$	ON	TN	$P\text{-}PO_4^{3-}$	OP	TP
V/R	0.1	3.2	0.4	0.5	0.3	49.0	1.2	31.9
V/inland waters	0.2	23.9	27.3	3.6	1.6	152.9	2.6	86.0
R/inland waters	1.3	7.5	73.0	7.0	4.7	3.1	2.2	2.7

Nutrient concentrations in Fonias surface and ground waters were low, consistent with the undisturbed nature of the basin (Skoulikidis et al., 2020) (Fig. 3b, Table S1b). Median (used for the purposes of the WFD) stream nitrate concentration (0.23 mg/l $N\text{-}NO_3$) was close to the high/good boundary (0.22 mg/l $N\text{-}NO_3$) of the HWQI. Springs revealed a similar median concentration of 0.20 mg/l $N\text{-}NO_3$. In the tributaries, the F-ds, the Ba spring and the vapor samples (including the long-term one) nitrate levels were less than 0.21 mg/l $N\text{-}NO_3$, whereas the rain samples illustrated a median value of 0.29 mg/l. Despite the high nitrite concentrations in all atmospheric samples (Fig. 3b, Table S1b), stream and spring concentrations were below or close to the LOQ (Table S1b). Ammonium showed also high levels in atmospheric samples, however stream and spring concentrations were very low (Fig 3b, Table S1b). Surface and groundwaters did not differ significantly regarding ON levels, with minimum values recorded in Am and It springs and maximum in F-ds (Fig. 3b, Table S1b). The ON% fraction in surface waters was variable, ranging between 7.7 % (F-us) and 59.4 % (2nd T) in streams and between 3.9 % (It) and 48.8 % (Ba) in springs.

All inland waters revealed a high orthophosphate and TP quality (Table S1b, Fig. 3b). The highest $P\text{-}PO_4$ concentrations were found in the springs, ranging from 0.003 (AA) to 0.017 (Ba) mg/l. In surface waters, orthophosphate concentrations ranged between 0.001 (2nd T) and 0.003 (F-us) mg/l $P\text{-}PO_4$. The highest OP concentration was at the Ba and AA springs and the 2nd T (0.005-0.007 mg/l) and the lowest at the Am and It springs, the F-us and F-ds, and the 1st T (0.002-0.004 mg/l). Finally, the OP% fraction was maximum at the 2nd T (78.8 %), followed by the Ba spring and F-ds (49.5 and 24.9 %, respectively), whereas It and Am springs and the F-us were characterized by low OP% (4-7.9 %) (Fig. 3b, Table S1b).

Contrary to the general trend in running waters (e.g. Skoulikidis, 2018; Skoulikidis et al., 2021), F-us was more enriched in most nutrients compared to F-ds, except of ON (Fig. 3b, Table S1b). After the rain event, streams and springs presented an increase in nitrate concentration (1.3 - 1.4 times), except of the 2nd T that revealed a nitrate decrease. The other nutrient species did not show any particular trends (Fig. 3b, Table S1b).

The N/P ($DIN/P\text{-}PO_4^{3-}$) ratio varied substantially both among the examined water cycle components and among samples of the same water cycle component, particularly regarding atmospheric samples (Table S1b). The average N/P ratio for streams was 134 and for springs 51 (median 118 and 19, respectively). Regarding surface waters, the 1st T p-r and F-us presented maximum N/P levels (232 and 264, respectively) and the 2nd T a minimum one (44). In the springs, the N/P ratio ranged between 3.9 (Ba) and 168 (AA) (Table S1b).

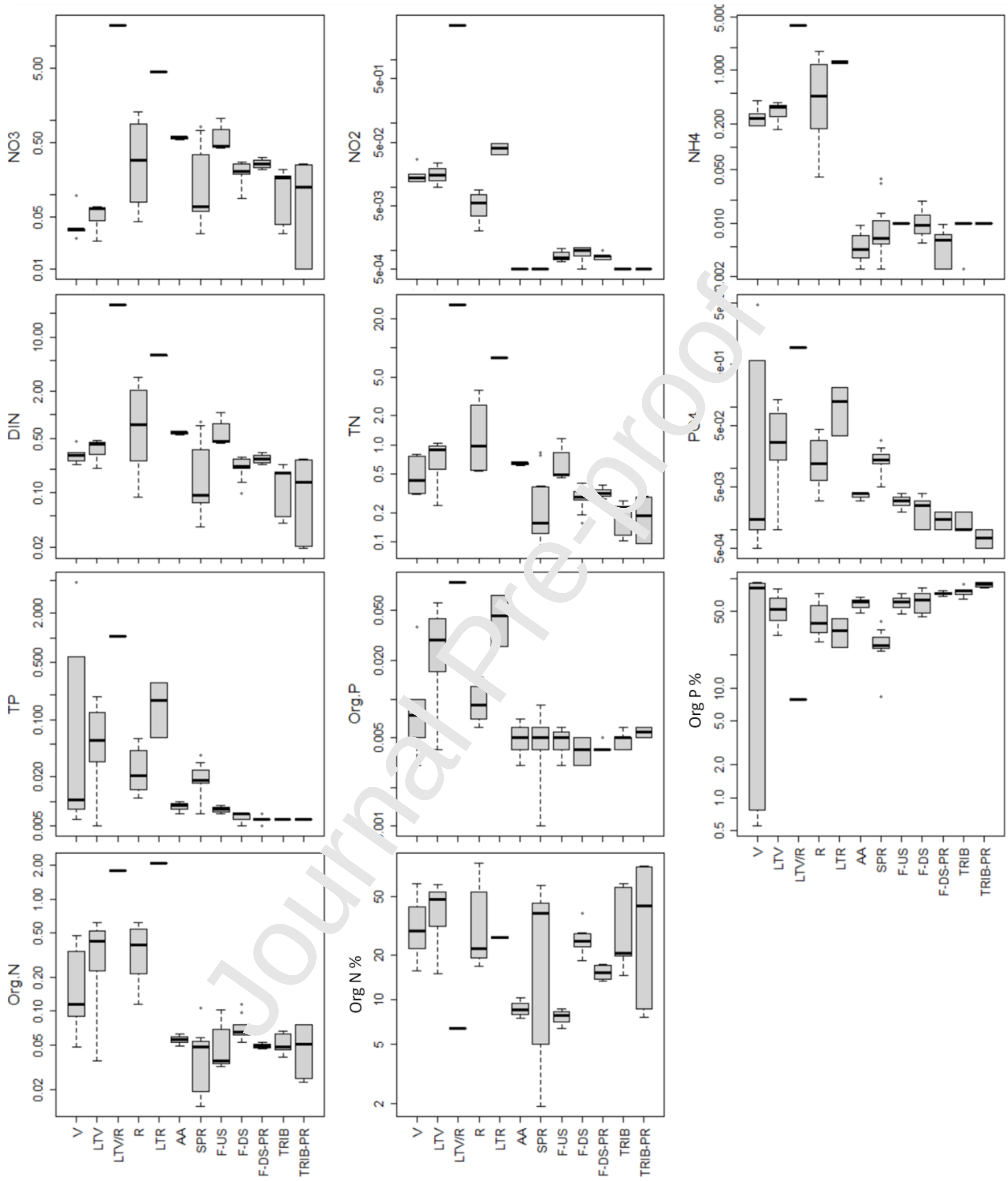

Figure 3b. Box plots of nutrient species' concentrations (mg/l) in the different aquatic systems examined. V: vapor samples, LTV: long-term vapor sample, LTV/R: long term vapor and rain sample, R: rain samples, LTR: long-term rain sample, AA: Agios Antonios spring samples, SPR: spring samples, F-US: Fonias upstream, F-DS: Fonias downstream, F-DS-PR: Fonias

downstream post rain, TRIB: tributaries, TRIB-PR: tributaries post-rain. Y-axis is in log scale. The AA spring was kept separately since it differed hydrogeologically from the other springs.

3.2.1.3 Stable isotopes

The $\delta^{18}O$ and $\delta^{2}H$ values in rain water samples ranged from -11.3 ‰ to 0.0 ‰ (average -5.5 ‰) and from -69.6 ‰ to -2.9 ‰ (average -36.8 ‰), respectively, whereas the LTR samples exhibited a more enriched isotopic composition (average -1.8 and -8.7 for $\delta^{18}O$ and $\delta^{2}H$, respectively) (Fig. 3c, Table S1c). The isotopic data in rainwater allowed producing a Local Meteoric Water Line (LMWL) similar to the Global Meteoric Water Line (GMWL) (Craig, 1961). The spring and stream water samples were plotted between the LMWL and the Eastern Mediterranean Water Line (EMWL) (Gat and Carmi, 1970) (Fig. S3). As expected, vapor and long-term vapor samples showed lower isotopic composition compared to rainwater samples, given that during evaporation vapor undergoes a negative enrichment opposite to the initial composition of water (Gonfiantini, 1986). In particular, the $\delta^{18}O$ and $\delta^{2}H$ values of the vapor samples ranged from -14.0 ‰ to -0.3 ‰ (average -7.1 ‰) and from -68.8 ‰ to -10.7 ‰ (average -31.9 ‰), respectively, whereas in the LTV samples the values were between -11.6 ‰ and -4.8 ‰ (average -9.1 ‰) for $\delta^{18}O$ and between -44.5 ‰ and -23.9 ‰ (average -35.9 ‰) for $\delta^{2}H$. The samples of the springs, the F-us and the tributaries showed similar $\delta^{18}O$ and $\delta^{2}H$ values (average ~-8.5 ‰ for $\delta^{18}O$ and ~-51.0 ‰ for $\delta^{2}H$), whereas the F-ds, including the post rain samples, exhibited a slightly enriched isotopic composition (on average -8.0 and -47.9 for $\delta^{18}O$ and $\delta^{2}H$, respectively). Most *d*-excess values of the rain water samples were lower than +10 ‰, whereas the terrestrial water samples averaged *d*-excess values ~+15‰.

We also examined the influence of the rain event that occurred on 22/9 in Ba spring, the tributaries and the F-ds sites for which post and prior to rain isotope values were available (Table S1d). The isotopic composition of the rain event was -9.9 ‰ and -64.6 ‰ for $\delta^{18}O$ and $\delta^{2}H$, respectively. The prior to rain period was from July till 20 September given that during this period no significant rain events occurred. The results showed that the $\delta^{18}O$ and $\delta^{2}H$ values in Ba spring slightly decreased from -8.5 ‰ and -49.8 ‰, prior to the rain event, to -8.7 ‰ and -51.2 ‰, after the rain event, respectively. Similarly the isotopic composition in the F-ds site slightly decreased from -7.9 ‰ ($\delta^{18}O$) and -47.6 ‰ ($\delta^{2}H$) to -8.1 ‰ and -48.1 ‰, respectively, and in the tributaries from -8.8 ‰ ($\delta^{18}O$) and -52.4 ‰ ($\delta^{2}H$) to -9.0 ‰ and -53.6 ‰, respectively.

The application of two end member mixing model (Eq. 1, 2) showed that the rain water of 22 September with $\delta^{18}O$ values lower than -9.0 % explained ~20±7 % of the isotopic composition of the Ba spring, ~31±17 % of the tributaries but only ~6±2 % of the F-ds.

The application of Equation 3 showed that the theoretical $\delta^{18}O$ values of the water vapor originating from the sea (-11.0 ‰) were closer to the observed ones (average LTV = -9.1 ‰) compared to the theoretical $\delta^{18}O$ values of the water vapor originating from the river (-20.5 ‰).

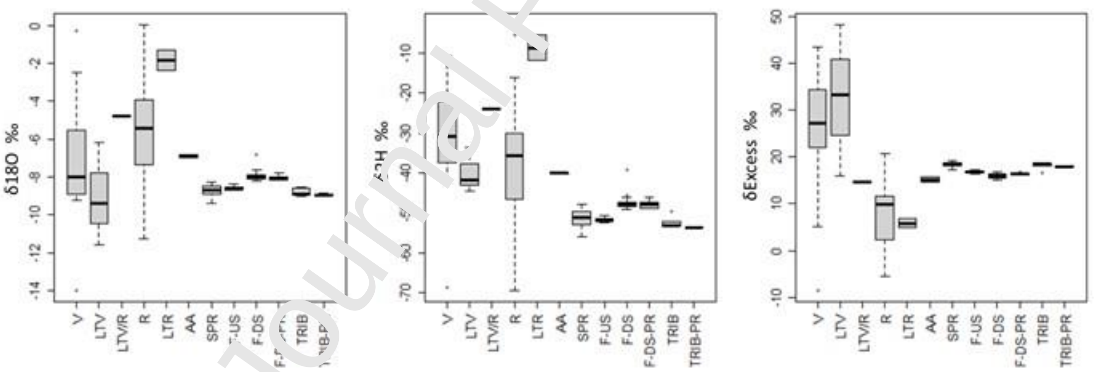

Figure 3c. Box plots of stable isotopes in the different aquatic systems examined. V: vapor samples, LTV: long-term vapor sample, LTV/R: long term vapor and rain sample, R: rain samples, LTR: long-term rain sample, AA: Agios Antonios spring samples, SPR: spring samples, F-US: Fonias upstream, F-DS: Fonias downstream, F-DS-PR: Fonias downstream post rain, TRIB: tributaries, TRIB-PR: tributaries post-rain. The AA spring was kept separately since it differed hydrogeologically from the other springs.

3.2.2. Element sources

Based on the EF values, the element's marine aerosol portion, both in surface and groundwaters, declined in the following order: Na^{+}>Mg^{2+}>K^{+}>SO_4^{2-}>>Ca^{2+}>>HCO_3^{-}>>Si, similarly to the long-term atmospheric samples (Table 2). On the average, the contribution of marine aerosol was higher for surface waters than for springs. The long-term atmospheric samples showed maximum affinity to marine aerosol, followed by the upstream springs and stream sites of the basin. Post rain samples showed variable response to marine aerosol inputs; increased inputs in F-ds and the 2nd T and mostly diminishing inputs in the Ba spring and in the 1st T.

Table 2. $EF_{seawater}$ for atmospheric samples, springs, and streams using Cl as reference element

	EF-Ca	EF-Mg	EF-Na	EF-K	EF-HCO_3	EF-SO_4	EF-Si
LTV/R	11.0	1.1	1.1	1.8	37	1.8	250
LTR	23.2	0.8	0.7	2.9	43	1.7	142
Am	46.4	1.7	1.2	4.4	263	4.0	41080
It	29.8	1.1	1.5	3.5	203	3.7	66174
Ba	80.5	4.2	1.4	3.6	534	3.2	70008
Ba p-r	79.6	4.3	1.5	3.7	441	3.3	72926
AA	195.3	4.1	1.4	3.2	755	9.2	33953
springs	**89.2**	**3.3**	**1.4**	**3.7**	**472**	**4.6**	**57709**
F-us	31.3	1.5	1.3	3.5	296	4.4	38592
1st T	28.4	1.7	1.2	2.3	294	3.3	45584
1st T p-r	31.3	2.0	1.3	3.7	310	3.3	46418
2nd T	25.5	1.4	1.2	1.5	263	2.7	41933
2nd T p-r	21.3	1.2	1.1	2.1	185	2.6	31894
F-ds	89.8	2.0	1.4	4.7	510	4.8	37809
F-ds p-r	68.8	1.9	1.3	4.6	365	4.8	36676

streams	**58.8**	**1.8**	**1.3**	**3.8**	**378**	**4.2**	**38970**

Table 3 presents an estimate of the contribution of wet deposition (rainfall and vapor), including sea spray and terrestrial portions (i.e. dust and/or atmospheric pollution), to inland waters' element concentrations according to the methodology described in section 2.2.3.2. Detailed results of this procedure are presented in Table S2.

Wet deposition to inland waters contributed over the half of sodium and sulfate and high portions of the rest of elements, besides silica. The contribution of rain to major ions and silica was far more significant compared to vapor, especially regarding sodium. With the assumption that 100% of chloride derives from marine aerosol (see section 2.2.3.2), over the half of sodium, and magnesium found in precipitation may be attributed to marine aerosol, whereas for silica, bicarbonate and calcium the contribution of terrestrial sources was significant (>95 %).

A Spearman correlation comparing the two methods applied to estimate marine aerosol contribution to inland waters' elemental concentrations, i.e., the EF (Table 2) and the mass-balance model (Table S2), showed satisfactory linear correlations; calcium (r=0.81), magnesium (r=0.87), sodium (r=0.40), potassium (r=0.80), bicarbonate (r=0.90), sulfate (r=0.90) and silica (r=0.84), for p<0.001.

In terms of the assumptions of the mass-balance model regarding the selection of dissolving salts and common silica phases, the utilization of PhreeQc software indicated that the stream and spring waters analyzed were undersaturated, and only quartz revealed slight oversaturation in over the half of the samples (Table S3). However, precipitation of quartz under non-pedogenic circumstances and the physicochemical conditions encountered is kinetically prohibited (Wilson, 2020). The activity diagrams employed to determine the hydrochemical composition of the examined stream and spring waters at the average temperature of 17°C revealed that the most likely clay mineral resulting from the weathering of silicate minerals is kaolinite, rather than various types of smectites and saponites (Fig. 4). This finding aligns with earlier studies on the weathering products of granitoid rocks (Banfield and Eggleton, 1988; 1990).

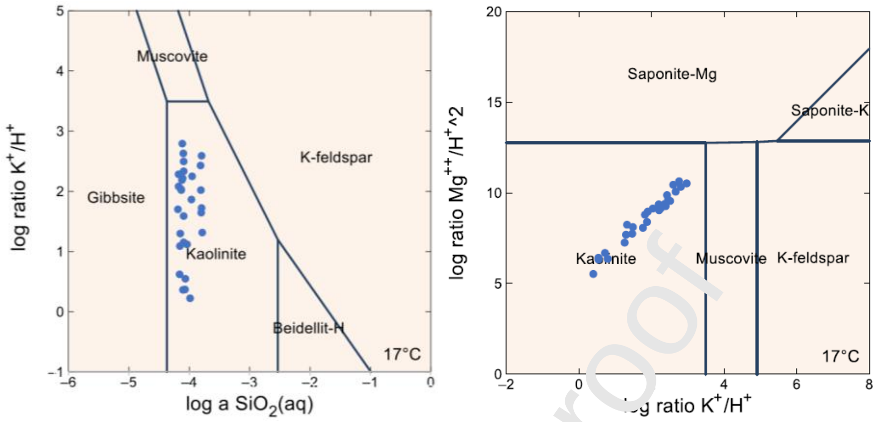

Figure 4. Activity diagrams a) log SiO_2 vs log K^+/H^+ (left) and b) log K^+/H^+ vs log Mg^{2+}/H^+ (right) with superimposed activity data from Fonias streams and tributaries calculated from hydrochemical data. Activity diagrams drown with Geochemist's Workbench and data points calculated with PhreeQc superimposed.

In Table 3 the portion of elements that derive from crustal sources, i.e. silicate mineral weathering and salt dissolution, according to the mass-balance model applied, compared to atmospheric inputs is presented. The detailed results of the model per site are presented in Table S4b. Compared to TDS, the average absolute modelled element error (remaining unbalanced elements after the model application) ranged between 0% (for silica) and 4.7% (for chloride). The average absolute sum of element errors was 8.9 % of TDS and ranged between 2.3 % for Ba and 20.7 % for the 2nd T p-r. When considering the concentrations in meq/l, the median TC-TA difference (total cations minus total anions) of the remaining ions after the model application was -0.009, whereas the median TC-TA difference of the precipitation corrected input data was -0.019 and for the measured data (prior precipitation correction) -0.027 (Tables S2, S3a). Median values were used to balance the high positive TC-

TA difference of the AA spring. Remaining TC-TA values after the model application correlated well with the TC-TA values of the precipitation corrected data (r=0.99, p<0.001). This evidence point out that the main source of the model error was caused by the analytical error.

According to Table 3, crustal processes contributed the vast majority of silica, and over the half of calcium, bicarbonate, potassium, magnesium and chloride to inland waters. Silica exclusively originated from silicate mineral weathering, whereas all the other elements chiefly derived from soluble salt dissolution.

Plagioclase, amorphous silica and biotite weathering contributed the vast portion of elements originating from silicate mineral weathering (Table 3). Potassium resulted primarily from biotite weathering; silica equally from amorphous silica and plagioclase; bicarbonate, sodium and calcium from plagioclase, whereas magnesium mainly derived from biotite weathering.

Considering salt dissolution, the vast portions of calcium and bicarbonate resulted from calcium carbonate dissolution; magnesium and sulfate derived chiefly from epsomite, while sodium and potassium chloride dissolution were the main sources of sodium, potassium and chloride (Table 3).

Table 3. Portion of marine aerosol and terrestrial sources in wet deposition. Portions of wet deposition (rainfall and vapor) and geogenic sources inputs (mineral weathering and salt dissolution), and of specific minerals and salts on the elements of inland waters in Fonias basin.

	Ca^{2+}	Mg^{2+}	Na^{+}	K^{+}	HCO_3^-	SO_4^{2-}	Cl^-	SiO_2
% of marine aerosol in wet deposition	4.74	62.63	62.25	40.26	0.40	20.30	100.00	0.02

% of terrestrial sources in wet deposition	95.26	37.37	37.75	59.74	99.60	79.70	0.00	99.98
% of rain in inland waters	21.50	33.20	59.90	30.10		53.40		3.60
% of vapor in inland waters	5.20	15.00	1.60	11.80		13.40		1.90
% of wet deposition in inland waters	**23.91**	**33.19**	**58.39**	**35.92**	**29.70**	**51.75**	**47.75**	**5.33**
% of wet deposition in streams	35.14	50.03	63.34	46.21	41.93	71.14	50.47	6.01
% of wet deposition in springs	29.09	28.88	55.02	30.30	30.00	51.26	46.58	4.78
% of lithological sources in inland waters	**76.09**	**66.81**	**41.61**	**64.08**	**70.30**	**48.25**	**52.25**	**94.67**
	Portion of mineral weathering/dissolution in inland waters							
Biotite weathering	0.00	6.58	0.00	19.17	4.53	0.00	0.00	3.19
Hornblende weathering	0.45	2.76	0.05	0.00	1.69	0.00	0.00	2.39
Plagioclase weathering	7.30	0.00	6.86	0.00	12.01	0.00	0.00	43.04
Orthoclase weathering	0.00	0.00	0.00	4.86	0.26	0.00	0.00	2.27
Amorphous silica weathering	0.00	0.00	0.00	0.00	0.00	0.00	0.00	43.79
NaCl dissolution	0.00	0.00	34.48	0.00	0.00	0.00	37.73	0.00
KCl disolution	0.00	0.00	0.00	37.47	0.00	0.00	2.85	0.00
$MgSO_4$ dissolution	0.00	39.7	0.00	0.00	0.00	43.2	0.00	0.00

		9				4		
$CaSO_4$ dissolution	1.80	0.00	0.00	0.00	0.00	5.01	0.00	0.00
$CaCO_3$ dissolution	57.13	0.00	0.00	0.00	49.12	0.00	0.00	0.00
$MgCO_3$ dissolution	0.00	3.57	0.00	0.00	1.48	0.00	0.00	0.00
Silicate weathering	**7.75**	**9.34**	**6.91**	**24.03**	**18.49**	**0.00**	**0.00**	**94.67**
Salt dissolution	**58.92**	**43.35**	**34.48**	**37.47**	**50.60**	**48.25**	**40.58**	**0.00**
Error	9.41	14.12	0.22	2.58	1.21	0.00	11.67	0.00

Table 4 illustrates the ratio between silicate weathering and salt dissolution portion contribution to the elements of the individual spring and stream sites examined, using the data of Table S4b. Upstream sites (headwater springs, F-us and the tributaries), revealed higher silicate mineral weathering contribution than downstream sites (AA and F-ds), where salt dissolution predominated.

Table 4. Ratio of silicate weathering versus salt dissolution contribution to each element for the stream and springs examined. Us: upstream sites (Am, Ba, F-us, 1st T and 2nd T), Ds: downstream sites (AA, F-ds).

	Ca^{2+}	Mg^{2+}	Na^{+}	K^{+}	HCO_3^{-}	SO_4^{2-}	Cl^{-}	Si
Am	0.25	0.21	0.38	0.24	0.74	0	0	1
Ba	0.13	0.09	0.24	0.41	0.26	0	0	1
AA	0.12	0.24	0.21	1	0.30	0	0	1
F-us	0.16	0.21	0.22	0.54	0.42	0	0	1
1st T	0.13	0.29	0.21	0.37	0.41	0	0	1

1st T p-r	0.18	0.67	0.26	2.02	0.49	0	0	1
2nd T	0.17	2.50	0.18	1	0.65	0	0	1
2nd T p-r	0.12	0.17	0.14	0.24	0.20	0	0	1
F-ds	0.06	0.11	0.13	0.26	0.25	0	0	1
F-ds p-r	0.02	0.03	0.08	0.23	0.07	0	0	1
Us	**0.16**	**0.29**	**0.24**	**0.88**	**0.45**	**0**	**0**	**1**
Ds	**0.06**	**0.09**	**0.12**	**0.24**	**0.17**	**0**	**0**	**1**

When correlating stream silica concentrations with TDS, two different trends were apparent; upstream sites (F-us, 1st and 2nd T) revealed a positive correlation (r=0.59, p<0.05), whereas for downstream sites (F-ds) the opposite trend was apparent (r=-0.57, p<0.05) (Fig. 5). Moreover, upstream sites revealed satisfactory positive correlations between silica and major ions, particularly with magnesium (r=0.94, p<0.001), calcium (r=0.79, p<0.01) and bicarbonate (r=0.68, p<0.05). On the contrary, downstream sites were marked by negative correlations between silica and major ions, particularly with calcium (r=-0.89, p<0.001), sodium (r=-0.68, p<0.05), magnesium (r=-0.60, p<0.05) and bicarbonate (r=-0.59, p<0.05).

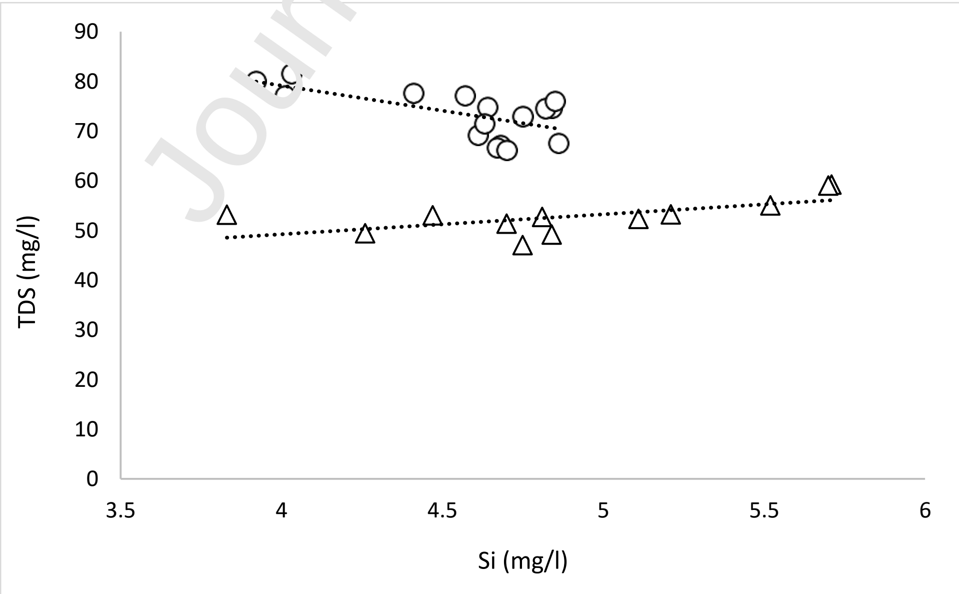

Figure 5. Linear regressions between silica and TDS concentrations (mg/l) for upstream (triangles) and downstream (cycles) stream sites

Element ratios in water are applied to track their possible sources (e.g., Mast et al., 1990; Gaillardet et al., 1999; Horton et al., 1999; Oliva et al., 2004). Table 5 presents the average element ratios of upstream and downstream spring and stream waters, the average element ratios in wet deposition used for the model, as well as the theoretical average element ratios of springs and streams that derive from silicate weathering and salt dissolution, according to the mass-balance model weathering and dissolution equations (Table S4a).

Table 5. Average ion ratios in upstream (Am, It, F-us, 1st and 2nd IT) and downstream (AA, F-ds) springs and stream waters, and in wet deposition, and theoretical average element ratios of springs and streams resulting purely from silicate weathering and salt dissolution according to the model. Us: upstream, Ds: downstream.

Element ratios	Us springs and streams	Ds springs and streams	Wet deposition	Silicate weathering (modelled)	Salt dissolution (modelled)
Ca^{2+}/Na^{+}	0.43	0.88	0.21	0.53	1.45
Ca^{2+}/Mg^{2+}	3.22	4.39	1.87	3.55	4.42
K^{+}/Na^{+}	0.05	0.07	0.03	0.51	0.00
Ca^{2+}/HCO_3^{-}	0.40	0.42	0.27	0.16	0.65
Mg^{2+}/HCO_3^{-}	0.13	0.10	0.14	0.04	0.12
Na^{+}/HCO_3^{-}	1.02	0.51	1.27	0.29	0.63

Upstream water ratios revealed higher affinity to wet deposition and silicate weathering ratios than downstream ones. In addition, downstream water element ratios were closer to salt dissolution ratios than upstream ones (Table 5).

The results of simper analysis (Table S5) based on groups formed in cluster analysis (Fig. S4), carried out major cations, sulfate and silica of atmospheric, spring and stream samples, distinguished six hydrochemical groups. The AA spring (group 1), presented the most distinct composition, compared to all other groups, mostly differentiating based on sulfate and calcium concentrations. The Ba spring (group 3) seemed to differentiate based on Si and Mg concentrations. The upstream spring and stream sites (group 5) and the F-ds sites (group 6) were the groups that accumulated the higher number of samples, with the lower differences between them. Groups 5 and 6 differentiated mainly based on potassium. The late rain events (group 4), presented similarities with the stream sites, while vapor and a June rain event (group 2) presented higher similarities with the Barrels spring (group 3). Similar groupings and simper results were obtained focusing exclusively on springs and streams when including all major ions and silica.

Focusing on nutrients, according to the cluster analysis groups (Fig. S5), streams and spring sites (groups 4 and 5) were similar (average group distance 0.08). The groups of atmospheric samples (groups 1,2 and 6-9) presented significant differences between them and from springs and streams. Even rain samples collected the same day but at different locations varied significantly. A vapor sample differed substantially from all other groups due to its high phosphate content. Finally, a number of vapor samples (group 3) presented higher similarities with springs and streams than rain.

4. Discussion

During the field work (i.e. 77 days), the total rainfall at 780 m asl was only 15 mm. At the same time, the mountainous part of the study area was covered several times by thick fog layers which promoted humidity, particularly during the night hours, when 20% of the hourly measurements exceeded 85% RH. Fog and scarce rain events were favored by strong and cold western winds, primarily W-NW and secondarily S-SW blowing. During the same time, water level measurements at the downstream portion of Fonias stream did not differed substantially. In contrast, marked diurnal fluctuations, with an average increase of 13 % during the night, are attributed to the combined action of evapotranspiration during the day and increased vapor condensation during the night. The stream water level increased short after the rain event of 22/9, along with the relatively quick recession of the hydrograph suggesting that the mountainous groundwater aquifers are confined, as previously assumed (Skoulikidis et al., 2020).

Regarding methodological aspects of the mass-balance model applied, the assumption that the ionic ratios of marine aerosol resemble to those of sea water is based on the evidence that major ion fractionation during the production of sea-salt aerosol is limited, if it occurs at all (Keene et al., 2007). The assumption that all chloride in wet deposition (rain plus vapor) derived from marine aerosol is considered likely since evaporite deposits are not present either in Samothraki nor in the broader area of Thrace region, whereas amphiboles and biotites may contribute only trace chloride amounts. The higher concentrations of calcium, magnesium and potassium in wet deposition compared to their minimum concentrations in inland waters are attributed to the fact that precipitation events during the period of sampling (predominately summer) were more enriched in elements than in the wet season due to higher atmospheric dust and anthropogenic inputs (Keresztesi et al., 2020). Thus, winter and spring precipitation events that enriched groundwater aquifers should have been less mineralized than those measured during the field work. Concerning the influence of small free grazing ruminants on major element mass balance, we assumed that elements taken out from plants by free grazing animals return in the form of excrements, thus the faunistic processes being most likely in a steady-state (Abe et al., 2019). The influence of vegetation in the particular watershed may be justifiably ignored, because there is only thin or lacking soil cover and related plant biomass (Drever and Hurcomb, 1986; Giovanoli et al., 1988, Bucher et al., 2017) and, in any case, may be considered in a steady state (i.e., elements uptake by the growth of any new vegetation is balanced by elements released from plant decay) (Drever and Clow, 1995; Likens and Bormann, 1994, Viers et al., 2005; Abe et al., 2019). Moreover, samplings took place in the dry season resulting in minor vegetation/water and soil/water element exchanges. Regarding in-stream biogeochemical processes that may potentially affect element composition, flashy flow regime of surface waters (Skoulikidis et al., 2020), combined with low in-stream productivity (Smeti et al., 2023) ensure minor influences. Finally, regarding cation-exchange soil processes, these are expected to be at steady-state since anthropogenic acid deposition in the study area is not occurring as the relatively high pH values of wet deposition confirm (Berner and Berner 1987; Drever and Clow, 1995; Viers et al., 2014), which exceed the pH of natural precipitation (5.5) (Tsagkaraki et al., 2020).

Compared to the most common Greek stream hydrochemical types (Skoulikidis et al., 2006), the predominating Fonias basin type (Ca^{2+}>Na^{+}>Mg^{2+}>K^{+} - HCO_3^->Cl^->SO_4^{2-}) is relatively uncommon, whereas the sodium bicarbonate type is rare. Compared to Greek rivers and streams (Skoulikidis, 2018), the average TDS concentration (incl. silica) in Fonias main stream and tributaries (64.7 mg/l) was almost six times lower. Considering the low (<1.5 meq/l) TC+TA (total cations plus total anions) concentrations of the sodium bicarbonate type samples found at the upstream portion of the basin (i.e. the 2nd T and the early summer samples of the 1st T and of F-us), these stream sites/samples can be termed as rain dominated, according to Meybeck (1981). To this type belong also the early summer samples of Am spring. Finally, the It spring, fitting in a sodium chloride type, with a TC+TA concentration of 0.92 meq/l, is a very rare, rain dominated hydrochemical type. In fact, the elements of these montane stream and spring sites were mostly affected by atmospheric inputs, as confirmed by the EFs (Table 2), the model results (Tables 4, S2) and the simper analysis (Table S5).

The isotopic results confirmed that the spring and stream waters in the basin are mainly recharged from rainwaters produced from Mediterranean air masses (Fig. S3), and particularly by those rain events with lower $\delta^{18}O$ and $\delta^{2}H$ values, whereas the isotopically more enriched rain events due to evaporation, show less contribution. The rain samples (R) showed similar average values for $\delta^{18}O$ and $\delta^{2}H$ compared to long-term data of isotopes in precipitation from Thessaloniki (Argiriou & Lykoudis 2006). However, the d-Excess value was lower in rain, also of long-term data from stations close by (Argiriou & Lykoudis 2006) compared to streams and springs indicating contributions of vapor as water source. The application of two end member mixing model when using $\delta^{18}O$ and $\delta^{2}H$ (Eq. 1, 2) showed that the rainfall event of 22 September predominately affected the upstream river basin and less the springs and the downstream part of the river. This is due to faster response of the upstream part to rain events.

Rain, vapor and long-term wet deposition samples ranged between a sodium and a calcium type, the latter being attributed to the dissolution of calcium carbonate rich dust particles. Low anthropogenic acid inputs combined with the neutralizing capacity of carbonate dust particles resulted to relatively high pH values in wet deposition. The EFs of LTR and LTV/R revealed a much stronger influence of marine aerosol on all elements, compared to inland waters (Table 2). Dissolution of dust and, especially, of sea salt particles during the time between sampling and sample collection of LTV/R and LTR initiated their significant enrichment in solutes. The origin of vapor (V) samples was evidenced by the isotopic values (Table S1c, Fig. 3c). The results of the mass balance model (Eq. 2) showed that the vapor is probably originating from the nearby sea. However, the possibility of a vapor origin from the local rivers cannot be excluded, in case secondary fractionation processes (e.g., evaporation) have altered the isotopic composition of the vapor. The low *d*-excess values (<10 ‰) in rain water samples were attributed to sub-cloud evaporation of rain drops, which is very common during the summer season in Mediterranean climates (Froehlich et al., 2008). The high *d*-excess values in vapor samples (> 20 ‰) were indicative of low relative humidity conditions at the oceanic moisture source (Pfahl and Sodemann, 2014). Similar *d*-excess values in vapor samples have been observed in the Mediterranean and elsewhere (e.g., Gat et al., 2003; Uemura et al., 2008).

Element concentrations in rain and vapor were in some cases lower and in others higher compared to other regions around the globe (Dollard et al., 1983; Sigg et al., 1987; Neal et al., 2003a,b; Beiderwieden et al., 2005; Blas et al., 2010; Budhavant et al., 2014; Giulianelli et al., 2014; Wang et al., 2019). Compared to European studies (Neal et al., 2003a,b; Blas et al., 2010; Giulianelli et al., 2014), Samothraki was far less enriched in vapor-related elements. Moreover, contrary to other studies (Neal et al., 2003a,b; Beiderwieden et al., 2005; Wang et al., 2019), vapor was less enriched with nitrate and ammonium than rain. In contrast, phosphate revealed significant enrichment in vapor relatively to rain compared to other regions (Neal et al., 2003a; Beiderwieden et al., 2005), illustrating however substantial variability among samples (Fig. 3b).

The low solute concentration of streams and headwater springs was attributed to the weathering resistant silicate nature and steep gradients of the basin with minimal soil development, causing low residence times and limited interaction between precipitation and minerals, both in the surface and the subsurface (Gibbs, 1970: Meybeck, 1983; Clow and Sueker, 2000; Skoulikidis et al., 2020); headwater springs and stream tributaries percolate rapidly through steep, V- shaped valleys, predominately covered with large rock debris, while the F-us is a bedrock type reach, receiving its water from springs and brooks of the same characteristics. The downstream rise in solute concentrations was attributed to increasing residence times of baseflow in lowland aquifers and more intense surface/ groundwater interactions (e.g. Skoulikidis, 2018). Moreover, the downstream increase of floodplains enhances salt flashing rates (Skoulikidis et al., 2006; Skoulikidis, 2018). This is consistent with the model results showing that salt dissolution dominates in the lower part of the basin (Tables 4, 5, S3).

Focusing on the impact of the rain event on stream and spring composition, post-rain diminishing of ion concentrations (e.g., in Ba spring and F-ds regarding calcium and hydrogen carbonate) were due to dilution, whereas increasing element concentrations (e.g., in the tributaries and partly in F-ds) where due to mineral/salt dissolution and flashing processes overwhelming dilution. Moreover, the downstream increase of floodplains enhances salt flashing rates (Skoulikidis et al., 2006; Skoulikidis, 2018). This is consistent with the model results showing that salt dissolution dominates in the lower part of the basin (Tables 4, 5, S3).

Regarding nutrients, nitrate was subject to post-rain flashing, indicating (in absence of any agrochemical pollution in the basin) natural organic matter mineralization and subsequent nitrification processes (Austin et al., 2004; Arce et al., 2014). Rapidly occurring post-rain nitrification processes may have triggered ammonium diminishing, contrary to other studies focusing on initial autumn flash floods (Skoulikidis and Amaxidis, 2009; Skoulikidis et al., 2017).

Wet deposition (rain and vapor) was the main sulfate and sodium source in inland waters and contributed significant portions of chloride and magnesium, with rain being much more important element contributor than vapor. Dust and, possibly, atmospheric CO_2 and SO_2 contribution, were the main sources of bicarbonate, calcium, sulfate and potassium in wet deposition, while dust and marine aerosol sources contributed equal portions of sodium and magnesium (Table 3). The high contribution of precipitation on the hydrochemical regime of Fonias stream has been confirmed for the hydrological network of the whole island (Skoulikidis et al., 2020), and is triggered by low solute concentrations. According to the model prescriptions, the lower the TDS concentration of the examined sites the higher was the atmospheric contribution. Thus, upstream sites, marked by low solute concentrations, presented a higher atmospheric element contribution (Tables 4, S3). However, this result is supported by following independent evidences; the upstream springs and stream sites were mostly affected by marine aerosol, as the EF values confirm (Table 2), spring and stream element ratios showed that upstream sites were more related to wet deposition compared to downstream sites (Table 5), whereas isotopic evidence confirmed the higher influence of the rain event at the upstream part of the basin compared to the downstream one, as described above. These evidences, along with the high positive correlations between the EF (where the interference of differing element concentrations among samples is well balanced) and the model results, justify the methodology applied for the specific TDS range of the examined catchment. Atmospheric contribution would be even more pronounced if we have considered dry deposition (Junge and Gustafson, 1957), being the dominant atmospheric deposition mechanism of particulate elements (Cheng et al., 2021).

Besides sodium and sulfate that were primarily of atmospheric origin, the other elements chiefly derived from bedrock lithology (Table 3). Silicate mineral weathering played a major role in delivering the main portion of silica to inland waters, and was more expressed at the upstream portion of the basin (Table 4). Soluble salt dissolution contributed the main portions of calcium, and bicarbonate to inland waters (Table 3) and was more intense at the downstream portion of the basin (Table 4). The differing upstream - downstream silicate weathering and salt dissolution intensity according to the model is supported by stream and spring element ratios; upstream water ratios revealed higher affinity to silicate weathering ratios than downstream ones, and downstream water ratios were closer to salt dissolution ratios than upstream ones (Table 5). The increase of the $\delta^{18}O$ and $\delta^{2}H$ values at the downstream sites are indicative of increasing water residence time favoring not only evaporation but also mineral dissolution. On the contrary, the positive correlations between silica versus TDS (Fig. 5) and major ions, illustrate the dominance of silicate mineral weathering at the upstream portion of the basin. On the other hand, the negative correlations between silica and major ions at the downstream portion of the basin could be explained by the fact that any acid inputs selectively boost soluble salt (e.g., carbonate) dissolution over silicate mineral weathering (Bufe et al., 2021).

On average, 85 % of calcium originating from crustal processes derived from $CaCO_3$ dissolution (Tables 3, S3b), despite the fact that the study area is a monolithological granitoid basin. However, intense physical weathering and erosion (Panagopoulos et al., 2019; Skoulikidis et al., 2020) expose fresh bedrock that may contain highly concentrated disseminated soluble salts in minor amounts which weather relatively quickly compared to silicate minerals (Garrels and Mackenzie, 1971; Drever, 1997; Horton et al., 1999; Clow and Sueker, 2000; Sun et al., 2018). In addition, calcium salts that accumulate during the dry season in soil pores may be flashed in the stream during flood events, particularly at the lowland portion of the basin (Moatar et al., 2017; Skoulikidis et al., 2017). Similarly, Mast et al. (1990) and Oliva et al. (2004) attributed 80 % of calcium in granite watersheds to trace calcic salt dissolution, the remaining 20% being assigned to silicate mineral weathering. As for calcium, geogenic elements originated primarily from salt dissolution, besides silica (Tables 3, S3b). Flashing of epsomite and gypsum during initial floods found in other Mediterranean basins (Skoulikidis and Amaxidis, 2009; Skoulikidis et al., 2017), points out towards salt accumulation processes in soil pores or rock cracks during hot and dry climatic conditions.

Main restrictions of the applied model include the fact that weathering and dissolution reactions in nature do not proceed sequentially but more or less simultaneously and not at the same rates (Bucher et al., 2017; Apollaro et al., 2021) and the assumption that only a fraction of the remaining potassium after biotite weathering derived from orthoclase weathering. The latter assumption grounds on the fact that orthoclase is markedly more resistant to weathering than the plagioclase (Banfield and Eggleton, 1990). In addition, it is expected that, like in the case of the other major ions, a portion of potassium ions derive from potassium salts' dissolution, e.g., sylvite, which may dissolve assuming undersaturation, dictated by the low potassium and chloride ions in the waters examined. Dissolution of KCl salt is supported by the higher positive correlation between potassium and chloride than between potassium and silica, and by the post-rain increase of both potassium and chloride. Finally, as pyrite has not been identified in the geological studies of Samothraki and the Fonias basin (Tsikouras, 1992; Seymour et al., 1996, Christophides et al., 2000), we did not consider it in the geochemical mass balance model, although its occurrence cannot be excluded and its oxidation and dissolution may result due to the high oxygen content of surface and ground waters. Nevertheless, despite the aforementioned shortcomings, the mass-balance model provided reasonable results, that were supported by independent evidences, considering the remarkably low solute concentrations in the basin that amplify the computational error, and the fact that the unbalanced ion concentrations remaining after the model application (Table S4a), mainly resulted from analytical errors.

In absence of any pollution sources in the basin, despite any impacts of free grazing animals, precipitation comprises a major source for dissolved nutrients. However, all nutrient species presented low concentrations in streams and springs, besides nitrate; overall, nutrient levels in surface waters were 1.2 (nitrate) to 6 (phosphate) times lower than the average of 163 high-quality stream sites of the national WFD network (Skoulikidis et al. 2021). The low nutrient concentrations, despite the significant inputs from wet deposition are attributed to effective immobilization/removal mechanisms within this undisturbed basin (Boon and Sorrell, 1991; Nihlgard et al,. 1994; Bernal et al., 2007) or in-stream (Triska et al., 1994; Costerton et al., 1995). According to Peterson et al. (2001), low to moderate inorganic N inputs to headwater streams are being effectively removed within minutes to hours and within small distances. Nitrate was relatively enriched in nearly pristine, mountainous sites (i.e. It spring and F-us), and departs from the high quality (according to the WFD) similarly to other upland streams and springs of the island (Skoulikidis et al., 2020). This may be attributed to the high mineralization and nitrification capacity of the headwaters (Peterson et al., 2001) and indicates that plants are not nitrogen-limited (Clow and Sueker, 2000), as the high stream N/P ratios show. Further downstream, within interfering pools and stream sections with low flow energy, nitrate concentration diminished possibly due to prevailing denitrification (Arce et al., 2015). Finally, mineralization processes of the accumulated atmospheric organic matter in the LTV/R sample resulted in a vast drop of ON and OP portions causing a phosphate rise and a dramatic nitrate increase, which by far exceeded stream and spring levels.

Conclusions

The study area, a small, nearly pristine, monolithological basin has been proved ideal for linking lithology, atmospheric inputs and stream chemistry. The model applied provided robust results that were supported by independent evidence (i.e., EF-values, element ratios and water stable isotopes) despite the low basin solute concentrations, the fact that weathering and dissolution reactions in reality do not proceed sequentially but more or less simultaneously and not at the same rates, and the assumption that only a fraction of orthoclase was subject to weathering. As the model results strongly depend on wet deposition composition, to optimize the results it is recommended in future studies to obtain dense data on rainfall and fog events. Water stable isotope applications revealed the contribution of vapor water to the water cycle of the basin. Inland waters showed clear chemical signatures of bedrock mineralogy and atmospheric inputs; weathering and dissolution of bedrock minerals and secondary salts contributed the main element portions, besides sulfate and sodium that chiefly derived from wet deposition, with rain being much more important element contributor than vapor. In wet deposition, terrestrial sources (dust and, possibly, atmospheric pollutants) were the main sources of bicarbonate, calcium, sulfate and potassium, whereas marine aerosol, being by definition the only source of chloride, was the main contributor of sodium and magnesium to inland waters. Weathering resistant bedrock, combined with steep slopes and flashy surface and subsurface flow regime, caused low solute concentrations in springs and streams, particularly at the upstream portion of the basin that was more affected by wet deposition chemistry and silicate mineral weathering than the lowland one. The downstream solute concentration increase was due to increasing water residence time favoring salt dissolution processes, that may have outpaced silicate mineral weathering reactions. The undisturbed character of the basin and effective self-purification processes were mirrored in low nutrient levels, despite the significant inputs from wet deposition. Rain was more important N-source contributor than vapor. However, phosphate may be significantly enriched in vapor relatively to rain compared to other regions. Relatively high nitrate concentrations were attributed to the increased mineralization and nitrification capacity of the headwaters, resulting in phosphorus-limited photosynthesis, while the downstream nitrate diminishing was ascribed to prevailing denitrification processes. This study highlights the importance of mass-balance model applications to estimate background levels of major elements in disturbed stream basins, thus contributing to stream basin reference conditions according to the WFD, as well as the need to estimate precipitation-related nutrient inputs, when carrying out pressure-impact assessments for aquatic ecosystems.

Acknowledgements

We are grateful to: Christina Papadaki for contributing to preliminary field work in summer 2020 and for providing the photo of Figure S1; Anastasia Lampou for creating the map of Figure 1 and calculating land uses in the basin; Stelios Valmas for maintaining the automatic monitoring stations and providing electronic advice for the active fog collector; Yiorgos Maskalidis, Giannis Pratikakis, Manolis Stergiou and Panayiotis Tsotoulidis for collecting rain and stream samples prior the actual field work; Dimosthenis Manzakis, Yiorgos Tarzan, Aggelos Tsiamis, Leonidas Soglemezis and Aggelos Akrida for guiding Saos-mountain campaigns and installing the harp-collector.

Funding: This work was supported by a HCMR self-funding project

References

Abe S.S., T. Harada, H. Okumura, T. Wakatsuki (2019). Comparing Rates of Rock Weathering and Soil Formation between Two Temperate Forest Watersheds Differing in Parent Rock and Vegetation Type. JARQ 53 (3). 169-179. DOI: 10.6090/jarq.53.169.

Amundson, R., D.D. Richter, G.S. Humphreys, E.G. Jobbaìgy, J.R.M. Gaillardet (2007). Coupling between biota and earth materials in the critical zone, Elements, 3, 327–332, https://doi.org/10.2113/gselements.3.5.327.

Antweiler R.C. (2015). Evaluation of Statistical Treatments of Left-Censored Environmental Data Using Coincident Uncensored Data Sets. II. Group Comparisons. Environ. Sci. Technol. 49, 13439–13446. https://doi.org/10.1021/acs.est.5b02385.

Apollaro C., I. Fuoco, L. Bloise, E. Calabrese, L. Marini, G. Vespasiano and F. Muto (2021). Geochemical Modeling of Water-Rock Interaction Processes in the Pollino National Park. Geofluids, Article ID 6655711. https://doi.org/10.1155/2021/6655711.

Arce, M., M.M. Sánchez-Montoya, M.R. Vidal-Abarca, M.L. Suárez, R. Gómez (2014). Implications of flow intermittency on sediment nitrogen availability and processing rates in a Mediterranean headwater stream. Aquat. Sci. 76, 173–186. DOI: 10.1007/s00027-013-0327-2.

Arce M., M.M. Sánchez-Montoya, R. Gómez (2015). Nitrogen processing following experimental sediment rewetting in isolated pools in an agricultural stream of a semiarid region. Ecol. Eng. 77, 233–241. http://dx.doi.org/10.1016/j.ecoleng.2015.01.035.

Argiriou, A.A. and Lykoudis, S., 2006. Isotopic composition of precipitation in Greece. Journal of Hydrology, 327(3-4), 486-495.

Austin A.T., L. Yahdjian, J.M. Stark, J. Belnap, A. Porporato, U. Norton, D.A. Ravetta, S.M. Schäffer (2004). Water pulses and biogeochemical cycles in arid and semiarid ecosystems. Oecologia 141, 221–235. https://www.jstor.org/stable/40005683.

Babulak S.W., L. Gildenberg (1973). Automated determination of silicate and carbonates in detergents. J. of the American Oil Chemists' Society, 50, 296-299. https://aocs.onlinelibrary.wiley.com/doi/abs/10.1007/BF02641359.

Banfield J.F., R.A. Eggleton (1988). Transmission Electron Microscope Study of Biotite Weathering. Clays and Clay Minerals, 36, 47-60. https://doi.org/10.1346/CCMN.1988.0360107.

Banfield J.F., R.A. Eggleton (1990). Analytical Transmission Electron Microscope Studies of Plagioclase, Muscovite, and K-Feldspar Weathering. Clays and Clay Minerals, 38(1), 77-89. https://doi.org/10.1346/CCMN.1990.0380111.

Beechie T.J., D.A. Sear, J.D. Olden, G.R. Pess, J.M. Buffington, H. Moir, P. Roni, M.M. Pollock (2010). Process-based Principles for Restoring River Ecosystems. BioScience 60: 209–222. doi:10.1525/bio.2010.60.3.7.

Beiderwieden E., T. Wrzesinsky, O. Klemm (2005). Chemical characterization of fog and rain water collected at the eastern Andes cordillera. Hydrol. Earth Sys. Sci. Discuss. 2, 863–885. www.copernicus.org/EGU/hess/hessd/2/863/

Bernal S., F. Sabater A. Butturini, E. Nin, S. Sabater (2007). Factors limiting denitrification in a Mediterranean riparian forest. Soil Biology & Biochemistry 39, 2685–2688. doi:10.1016/j.soilbio.2007.04.027.

Berner R.A., A.C. Lassaga, R.M. Garrels (1983). The carbonate-silicate geochemical cycle and its effect on atmospheric carbon-dioxide over the past 100 million years. Am. J. Sci. 283, 641–683. https://doi.org/10.2475/ajs.283.7.641

Berner E.K., R.A. Berner (1987). The Global Water Cycle. Prentice-Hall, Englewood Cliffs, NJ. ISBN 9780133571950, 0133571955.

Blarasin M., A. Cabrera, I. Matiatos, V. Lutri, L. Maldonado, D. Giacobone, E. Matteoda, F. Becher Quinodoz, J. Giuliano Albo, J., C. Eric, J. Felizzia (2020). Application of isotope techniques to enhance the conceptual hydrogeological model and to assess groundwater sustainability in the Pampean plain in Córdoba, Argentina. Isotopes in Environmental and Health Studies, 56(5-6), pp.402-417. https://doi.org/10.13140/RG.2.2.18888.34565.

Blas M., Z. Polkowska, M. Sobik, K. Klimaszewska, K Nowinski, J. Namiesnik (2010). Fog water chemical composition in different geographic regions of Poland. Atmos. Res. 95, 455-469. https://doi.org/10.1016/j.atmosres.2009.11.008.

Boltz D.F., M.G. Mellon (1948). Spectrophotometric determination of phosphate as molydiphosphoric acid, Analytical Chemistry, 20(8), 749-751. https://doi.org/10.1021/ac60020a021.

Boon, P.I., B.K. Sorrell (1991). Biogeochemistry of billabong sediments. I. The effect of macrophytes. Freshwater Biology 26, 209–226. https://doi.org/10.1111/j.1365-2427.1991.tb01730.x.

Brady J., S. College, D. Perkins (2022). Mineral Formulae Recalculation. University of North Dakota.https://serc.carleton.edu/research_education/equilibria/mineralformulaerecalculation.html (accessed 12.11.2022).

Bricker O.P., B.F. Jones, C.J. Bowser (2003). Mass-balance approach to interpreting weathering reactions in watershed systems. In: Holland, H.D., Turekian, K.K. (Ex. Eds.), Drever, J.I. (Ed.), Treatise on Geochemistry, vol. 5, Surface and Ground Water, Weathering, and Soils, Elsevier, New York, pp. 119–132. DOI: 10.1002/esp.3373.

Bricker O., B. Katz, A. Afifi, L. Puckett, C. Olson, M. Kennedy (1983). Geochemistry of small Appalachian watersheds developed on silicate bedrock. Sci. Geol. Bull. Mem. 73, 41–52.

Bucher K., W. Zhou, I. Stober (2017). Rocks control the chemical composition of surface water from the high Alpine Zermatt area (Swiss Alps). Swiss J Geosci 110, 811–831. DOI 10.1007/s00015-017-0279-y.

Budhavant K., P. Rao, P. Safai, L. Granat, H. Rodhe (2014). Chemical composition of the inorganic fraction of cloud-water at a high-altitude station in West India. Atmos. Environ. 88, 59‑65, http://urn.kb.se/resolve?urn=urn:nbn:se:su:diva-101085.

Bufe A., N. Hovius, R. Emberson, J.K.C. Rugenstein, A. Galy, H.J. Hassenruck-Gudipati, J.-M. Chang (2021). Co-variation of silicate, carbonate and sulfide weathering drives CO_2 release with erosion. Nature Geoscience, 14, 211–216. https://doi.org/10.1038/s41561-021-00714-3.

Cheng I., A. Al Mamun, L. Zhang (2021). A synthesis review on atmospheric wet deposition of particulate elements: scavenging ratios. solubility. and flux measurements. Environmental Reviews. https://doi.org/10.1139/er-2020-0118.

Christofides G., G. Eleftheriadis, J. Esson, T. Soldatos, A. Koroneos, M. Broecker (2000). The evolution of the Samothraki granitic pluton (N. Aegean, Greece): geochronology, chemical and isotopic constrains for AFC modelling. Proceedings of the 3rd Intern. Conf. on the Geology of the Eastern Mediterranean, 193-209.

Clark I.D., P. Fritz (1997). Environmental isotopes in hydrogeology. CRC press. ISBN 9781566702492.

Clark, K.R., R.N. Gorley (2006) PRIMER v6: User Manual/Tutorial (Plymouth Routines in Multivariate Ecological Research). PRIMER-E, Plymouth.

Cleaves E.T., A.E. Godfrey, O.P. Bricker (1970). Geochemical balance of a small watershed and its geomorphic implications. Geol. Soc. Am. Bull. 81, 3015–3032. https://doi.org/10.1130/0016-7606(1970)81[3015:GBOASW]2.0.CO;2

Clow D.W., J.K. Sueker (2000). Relations between basin characteristics and stream water chemistry in alpine/subalpine basins in Rocky Mountain National Park. Colorado. Water Resour. Res. 36, 49–61, https://doi.org/10.1029/1999WR900294.

Collett Jr.J.L., A. Bator, D.E. Sherman, K.F. Moore, K.J. Hoag, B.B. Demoz, X. Rao, J.E. Reilly (2002). The chemical composition of fogs and intercepted clouds in the United States. Atmospheric Research 64, 29-40.

Conway E.J. (1942). Mean geochemical data in relation to oceanic evolution. Proc. Roy. Irish Acad. 48, 119-159.

Costerton J.W., Z. Lewandowski, D.E. Caldwell, D.R. Korbrer, H.M. Lapin-Scott (1995). Microbial biofilms. Annual Review of Microbiology 49, 711–745. doi: 10.1146/annurev.mi.49.100195.003431.

Craig, H. (1961). Isotopic variations in meteoric waters. Science, 133(3465), 1702-1703. DOI: 10.1126/science.133.3465.170.

Dansgaard, W. (1964). Stable isotopes in precipitation. Tellus, 16(4), pp.436-468. https://doi.org/10.1111/j.2153-3490.1964.tb00181.x.

De Jong C., M. Mundelius, K. Migała (2005). Comparison of Evapotranspiration and Condensation Measurements between the Giant Mountains and the Alps. In de Jong, D. Collins and R. Ranzi (eds.) Climate and Hydrology in Mountain Areas. C.. John Wiley & Sons, Ltd., 161-183. DOI: 10.1002/0470858249.ch12.

Dessert C., B. Dupre, J. Gaillardet, L.M. Francois, C.J. Allegre (2003). Basalt weathering laws and the impact of basalt weathering on the global carbon cycle. Chem. Geol. 202(3–4), 257–273. DOI: 10.1016/j.chemgeo.2002.10.001.

Dollard G.J., M.H. Unsworth, M.J. Harve (1983). Pollutant transfer in upland regions by occult precipitation. Nature 302, 241‑243. DOI 10.1038/302241a0.

Dotsika, E., Lykoudis, S. and Poutoukis, D. (2010). Spatial distribution of the isotopic composition of precipitation and spring water in Greece. Global and Planetary Change, 71(3-4), pp.141-149.

Drever J.I. (1997). Weathering processes. In O. M. Saether and P. De Caritat (eds.) Geochemical Processes, Weathering and Groundwater Recharge in Catchments. Swets and Zeitlinger, 3–19. ISBN 9789054106463.

Drever J.I., D.R. Hurcomb (1986). Neutralization of atmospheric acidity by chemical weathering in an alpine drainage basin in the North Cascade Mountains. Geology 14 (3), 221–224. https://doi.org/10.1130/0091-7613(1986)14<221:NOAABC>2.0.CO;2.

Drever J.I., D.W. Clow (1995). Weathering rates in catchments. In: A.F. White and S.L. Brantley (eds.) Chemical Weathering Rates of Silicate Minerals. Reviews in Mineralogy, Vol. 31, pp. 463–481. ISBN 0-939950-38-3; ISBN13 978-0-939950-38-6.

European Environment Agency (EEA) (2020). Corine Land Cover 2018 – version 2020_20u1, Raster Data. Available online: https://land.copernicus.eu/pan-european/corine-land-cover/clc2018 (accessed on 10 May 2020).

European Environment Agency (EEA) (2018). European Waters, Assessment of Status and Pressures; EEA Report; Publications Office of the European Union: Luxembourg, p. 85.

Fischer D.T., C.J. Still (2007). Evaluating patterns of fog water deposition and isotopic composition on the California Channel Islands. Water Resources Research 43:W04420. DOI: 10.1029/2006WR005124.

Freyssinet P., A.S. Farah (2000). Geochemical mass balance and weathering rates of ultramafic schists in Amazonia. Chemical Geology 170 2000 133–151. DOI: 10.1016/S0009-2541(99)00245-4.

Froehlich K., M. Kralik, W. Papesch, D. Rank, H. Scheifinger, W. Stichler (2008). Deuterium excess in precipitation of Alpine regions–moisture recycling. Isotopes in Environmental and Health Studies 44(1), 61-70. https://doi.org/10.1080/10256010801887208.

Furman T., P. Thompson B. Hatchl (1998). Primary mineral weathering in the central Appalachians: a mass balance approach. Geochim. Cosmochim. Acta 62, 2889–2904. DOI: 10.1016/S0016-7037(98)00202-6.

Gaillardet J., B. Dupre, P. Louvat, C.J. Allegre (1999). Global silicate weathering and CO consumption rates deduced from the chemistry of large rivers. Chemical Geology 159, 3–30. https://doi.org/10.1016/S0009-2541(99)00031-5

Garrels R.M., F.T. Mckenzie (1971). Evolution of sedimentary rocks. W. W. Norton & Co. New York. 397 p. https://doi.org/10.4319/lo.1972.17.1.0165.

Garrels R.M., F.T. Mckenzie (1967). Origin of the chemical compositions of some springs and lakes. Advances in Chemistry Series 67. 222-242. DOI: 10.1021/ba-1967-0067.ch010.

Gat, J.R. and Carmi, I. (1970). Evolution of the isotopic composition of atmospheric waters in the Mediterranean Sea area. Journal of Geophysical Research, 75(15), 3039-3048. DOI: 10.1029/JC075i015p03039.

Gibbs R.J. (1970) Mechanisms controlling world water chemistry. Science 170, 1088-1090. http://www.jstor.org/stable/1730827

Giulianelli L., S. Gilardoni, L. Tarozzi, M. Rinaldi, S. Decesari, C. Carbone, M.C. Facchini, S. Fuzzi (2014). Fog occurrence and chemical composition in the Po valley over the last twenty years. Atm. Env. 98, 394-401. http://dx.doi.org/10.1016/j.atmosenv.2014.08.080.

Giovanoli R., J.L. Schnoor, L. Sigg, W. Stumm, J. Zobris (1988). Chemical weathering of Crystalline Rocks in the catchment area of Acidic Ticino Lakes. Switzerland. Clays And Clay Minerals 36(6), 521-529. https://www.dora.lib4ri.ch/eawag/islandora/object/eawag:2641.

Goldich S.S. (1938) A study of rock weathering. J. Geol. 46, 17–58. https://www.journals.uchicago.edu/doi/abs/10.1086/624619.

Gonfiantini, R. (1986). Environmental isotopes in lake studies. Handbook of Environmental Isotope Geochemistry; The Terrestrial Environment, pp. 113–168.

Gorham E. (1958). The influence and importance of daily weather conditions in the supply of chloride, sulfate and other ions to fresh waters from atmospheric precipitation: Royal Soc. London Philos. Trans., B, 247, 147-178. DOI 10.1098/rstb.1958.0001

Harmon R.S., W.B. Lyons, C.B. Gardner, S.T. Goldsmith, D.T. Long, H. Mitasova, S. Welch, K. Welch (2013). Surface water geochemistry and chemical weathering across Panama. Procedia Earth and Planetary Science 7. 342 – 345. doi: 10.1016/j.proeps.2013.03.134.

Harrell F.E. Jr (2022). Hmisc: Harrell Miscellaneous. R package version 4.7-2. https://CRAN.R-project.org/package=Hmisc.

HCP. CRC Handbook of Chemistry and Physics John R. Rumble (ed.). 103rd Edition. https://hbcp.chemnetbase.com/faces/contents/ContentsSearch.xhtml. accessed 15.10.2022.

Heiling C. (2018). On the state of oak forests in Samothraki: Tree regeneration, restoration priorities and forest structure as a mirror of past land use on a Greek island. Master Thesis, Institute of Forest Ecology, University of Natural Resources and Life Sciences, Vienna, Austria.

Hering, D., Á. Borja, J. Carstensen, L. Carvalho, M. Elliott, C.K. Feld, A.-S. Heiskanen, R.K. Johnson, J. Moe, D. Pont, A.L. Solheim, W. van de Bund (2010). The European Water Framework Directive at the age of 10: A critical review of the achievements with recommendations for the future. Sci. Total. Environ. 2010, 408, 4007–4019. doi: 10.1016/j.scitotenv.2010.05.031.

Hilberg, S., F. Riepler (2016). Interaction of various flow systems in small alpine catchments: conceptual model of the upper Gurk Valley aquifer, Carinthia, Austria. Hydrogeology Journal 24, 1231–1244. https://doi.org/10.1007/s10040-016-1396-9.

Horton T.W., C.P. Chamberlain, M. Fantie, J.D. Blum (1999). Chemical weathering and lithologic controls of water chemistry in a high-elevation river system: Clark's Fork of the Yellowstone River, Wyoming and Montana. Water Resources Research 35, 5, 1643-1655. DOI:10.1029/1998WR900103.

Junge, C.E., P. E., Gustafson (1957). On the distribution of sea salt over the United States and its removal by precipitation: Tellus, v. 9, p. 164-173. DOI: 10.3402/tellusa.v9i2.9092.

Katz B.G., O.P. Bricker, M.M. Kennedy (1985). Geochemical mass-balance relationships for selected ions in precipitation and stream water, Catoctin Mountains, Maryland. Am. J. Sci. 285, 931–962. https://doi.org/10.2475/ajs.285.10.931.

Kakiuchi M., S. Matsuo (1979). Direct measurements of D/H and 18O/16O fractionation factors between vapor and liquid water in the temperature range from 10 to 40 C. Geochemical Journal, 13(6), pp.307-311.

Keene W.C., H. Maring, J.R. Maben, D.J. Kieber, A.A.P. Pszenny, E.E. Dahl, M.A. Izaguirre, A.J. Davis, M.S. Long, X. Zhou, L. Smoydzin, R. Sander (2007). Chemical and physical characteristics of nascent aerosols produced by bursting bubbles at a model air-sea interface. Journal of Geophysical Research 112, D21202. doi:10.1029/2007JD008464.

Kendall C., E.A. Caldwell (1998). Fundamentals of Isotope Geochemistry. In C. Kendall and J. J. McDonnell (eds.) Isotope Tracers in Catchment Hydrology. Elsevier Science B.V., Amsterdam. ISBN: 9780444501554 pp. 51-86.

Keresztesi Á., M.-V. Birsan, I.-A. Nita, Z. Bodor, R. Szép (2019). Assessing the neutralisation, wet deposition and source contributions of the precipitation chemistry over Europe during 2000–2017. Environ. Sci. Eur. 31, 50. https://doi.org/10.1186/s12302-019-0234-9.

Keresztesi A., I.-A. Nita, R. Boga, M.-V. Birsan, Z. Bodor, R. Szep (2020). Spatial and long-term analysis of rainwater chemistry over them conterminous United States. Environmental Research 188, 109872. https://doi.org/10.1016/j.envres.2020.109872.

Kerouel R., A. Aminot (1997). Fluorometric determination of ammonia in sea and estuarine waters by direct segmented flow analysis, Marine Chemistry 57, 265-275. https://doi.org/10.1016/S0304-4203(97)00040-6.

Leake B.E., A. Woolley, C.E.S. Arps, W.D. Birch, M.C. Gilbert, J.D. Grice, F.C. Hawthorne, H.J. Kisch, A. Kato, V.G. Krivovichev, K. Linthout, J. Laird, J.A. Mandarino, W. Maresch, E.H. Nickel, N.M.S. Rock, J. Schumacher, D.C. Smith, N.C.N. Stephenson, L. Ungaretti, E.J.W. Whittaker, G. Youzhi (1997). Nomenclature of Amphiboles: Report of the Subcommittee on Amphiboles of the International Mineralogical Association, Commission on New Minerals And Mineral Names. The Canadian Mineralogist 35, 219-246.

Li X., G. Han, M. Liu, K. Yang, J. Li (2019). Hydro-Geochemistry of the River Water in the Jiulongjiang River Basin, Southeast China: Implications of Anthropogenic Inputs and Chemical Weathering. Int. J. Environ. Res. Public Health 16, 440; doi:10.3390/ijerph16030440.

Li Y., F. Aemisegger, A. Riedl, N. Buchmann, W. Eugster (2020). The role of dew and radiation fog inputs in the local water cycling of a temperate grassland in Central Europe. Hydrology and Earth Systems Science. https://doi.org/10.5194/hess-2020-493.

Likens G.E., F.H. Bormann (1994). Biogeochemistry of a Forested Ecosystem, 2nd edn. Springer, Berlin.

Mast M.A., J.I. Drever, J. Baron (1990). Chemical weathering in the Loch Vale watershed, Rocky Mountain National Park, Colorado. Water Resour. Res. 2612, 2971–2978. https://doi.org/10.1029/WR026i012p02971.

McClain, M. E., Boyer, E. W., Dent, C. L., Gergel, S. E., Grimm, N., Groffman, P. M., Hart, S. C., Harvey, J. W., Johnston, C. A., Mayorga, E., McDowell, W. H., & Pinay, G. (2003). Biogeochemical Hot Spots and Hot Moments at the Interface of Terrestrial and Aquatic Ecosystems. Ecosystems, 6(4), 301-312. https://doi.org/10.1007/s10021-003-0161-9.

Matiatos I., L.I. Wassenaar (2019). Stable isotope patterns reveal widespread rainy-period-biased recharge in phreatic aquifers across Greece. Journal of Hydrology 568, 1081-1092. DOI:10.1016/J.JHYDROL.2018.11.053.

Matiatos, I., A. Alexopoulos, A. Godelitsas (2014). Multivariate statistical analysis of the hydrogeochemical and isotopic composition of the groundwater resources in northeastern Peloponnesus (Greece). Science of the Total Environment 476, 577-590. https://doi.org/10.1016/j.scitotenv.2014.01.042.

Meybeck M. (2003). Global analysis of river systems: from Earth system controls to Anthropocene syndromes. Phil. Trans. R. Soc. Lond. B. DOI 10.1098/rstb.2003.1379.

Meybeck M. (1996). River water quality. Global ranges, time and space variabilities, proposal for some redefinitions. Verh. Internat. Verein. Limnol., 26, 1, 81-96. https://doi.org/10.1080/03680770.1995.11900694.

Meybeck M. (1983). Dissolved loads of Rivers and Surface Water Quantity/Quality Relationships. 1AHS Publ, no. 141. Atmospheric inputs and river transport of dissolved substances. Proceedings of the Hamburg Symposium, August 1983.

Meybeck M. (1981). Pathways of major elements from land to ocean through rivers. In: Martin JM, Burton JD, Eisma D, (editors) River inputs in ocean systems Proceedings of a

SCOR/ACMRR/ ECOR/ IAHS/ UNESCO/ CMG/ IABO/ IAPSO. Review and Workshop, 26–30 March 1979, Rome, Italy, 18–30.

Miller W.R., J.I. Drever (1977). Chemical weathering and related controls on surface water chemistry in the Absaroka Mountains, Wyoming. Geochimica et Cosmochimica Acta, 41, 1693-1702. https://doi.org/10.1016/0016-7037(77)90201-0.

Moatar, F., B.W. Abbott, C. Minaudo, F. Curie, G. Pinay (2017), Elemental properties, hydrology, and biology interact to shape concentration-discharge curves for carbon, nutrients, sediment, and major ions, Water Resour. Res., 53, 1270–1287, doi:10.1002/2016WR019635.

NASA (2022). National Aeronautics and Space Administration https://worldview.earthdata.nasa.gov. Accessed 20.9.2022.

Navone R. (1964). Proposed method for nitrate in potable waters, Amer. J., Water works Ass. 56, 781. DOI:10.1002/J.1551-8833.1964.TB01270X.

Neal C., B. Reynolds, M. Neal, S. Hughes, H. Wickham, L. Hill, P. Rowland, B. Pugh (2003a). Soluble reactive phosphorus levels in rainfall, cloud water, throughfall, stemflow, soil waters, stream waters and groundwaters for the Upper River Severn area, Plynlimon, mid Wales. The Science of the Total Environment 314–316, 99–120. doi:10.1016/S0048-9697(03)00099-8.

Neal C., B. Reynolds, M. Neal, L. Hill, H. Wickham, B. Pugh (2003b). Nitrogen in rainfall, cloud water, throughfall, stemflow, stream water and groundwater for the Plynlimon catchments of mid-Wales. Sci Total Environ 314-316, 121-51. doi: 10.1016/s0048-9697(03)00100-1.

Nihlgard, B.J., W.T. Swank, M.J. Mitchell (1994). Biological processes and catchment studies. In: Moldan, B., Cherny, J. (Eds.), Biogeochemistry of Small Catchments: A Tool for Environmental Research, SCOPE 51. John Wiley & Sons Ltd., pp. 133–161. Corpus ID: 128838797.

Noll N., C. Lauk, V. Gaube, D. Wiedenhofer (2020). Caught in a Deadlock: Small Ruminant Farming on the Greek Island of Samothrace. The Importance of Regional Contexts for Effective EU Agricultural Policies. Sustainability, 12, 762. doi:10.3390/su12030762.

Oliva P., B. Dupre, F. Martin, J. Viers (2004). The role of trace minerals in chemical weathering in a high elevation granitic watershed (Estibere, France): chemical and mineralogical evidence. Geochim. Cosmochim. Acta 68, 2223–2244. DOI: 10.1016/j.gca.2003.10.043.

Panagopoulos Y., E. Dimitriou, N. Skoulikidis (2019). Vulnerability of a Northeast Mediterranean Island to Soil Loss. Can Grazing Management Mitigate Erosion? Water, 11, 1491. https://doi.org/10.3390/w11071491.

Panagopoulos, Y., D. Alexakis, N. Skoulikidis, S. Laschou, A. Papadopoulos, E. Dimitriou (2022). Implementing the CCME Water Quality Index for theEvaluation of the Physicochemical Quality of Greek Rivers. Water, 14, 2738. https://doi.org/10.3390/w14172738.

Peterson B.C., W.M. Wollheim, P.J. Mulholland, J.R. Webster, J.L. Meyer, J.L. Tank, E. Marti, W.B. Bowen, N.M. Valett, A.E. Hershey, W.H. McDowell, W.K. Dodds, S.K. Hamilton, S/ Gregory, D.D. Morrall (2001). Control of nitrogen export from watersheds by headwater streams. Science, 292, 86-90. DOI: 10.1126/science.1056874.

Pfahl, S. and Sodemann, H., 2014. What controls deuterium excess in global precipitation?. Climate of the Past, 10(2), pp.771-781. https://doi.org/10.5194/cp-10-771-2014

Price J.R., K.C. Rice, D.W. Szymanski (2012). Mass-balance modeling of mineral weathering rates and CO_2 consumption in the forested, metabasaltic Hauver Branch watershed, Catoctin Mountain, Maryland, USA. Earth Surf. Process. Landforms. DOI: 10.1002/esp.3373.

R Core Team (2020). R: A language and environment for statistical computing. R Foundation for Statistical Computing, Vienna, Austria. URL https://www.R-project.org/

Raimbault, P., W. Pouvesle, F. Diaz, N. Garcia, R. Sempere, (1999). Wet oxidation and automated colorimetry for simultaneous determination of organic carbon, nitrogen and phosphorus dissolved in seawater. Marine Chemistry 66, 161-169. https://doi.org/10.1016/S0304-4203(99)00038-9.

Rao P.S.P., S. Tiwari, J..L. Matwale, S. Pervez, P. Tunved, P.D. Safai, A.K. Srivastava, D.S. Bisht, S. Singh, P.K. Hopke (2016) Sources of chemical species in rainwater during monsoon and non-monsoonal periods over two mega cities in India and dominant source region of secondary aerosols. Atmos Environ 146:90–99. https://doi.org/10.1016/j.atmosenv.2016.06.069.

Schofield R., D.S.G. Thomas, M. J. Kirkby (2001). Causal Processes of Soil Salinization in Tunisia. Spain and Hungary. Land Degrad. Develop. 12. 163-181. DOI: 10.1002/ldr.446.

Seymour K.St., V. Tsikouras, K. Kotopouli, K. Hatzipanayiotou, G. Pe-Piper (1996). A window to the operation of microplate tectonics in the Tethys Ocean: the geochemistry of the Samothrace granite, Aegean Sea. Mineralogy and Petrology 56, 251-272. https://link.springer.com/article/10.1007/BF01162606.

Sigg L., W. Stumm, J. Zobrist, F. Zurcher (1987). The Chemistry of Fog: Factors Regulating its Composition. CHIMIA 41, 5, 159-165. DOI: 10.1002/chin.198747400.

Skoulikidis N. (2018). The State and Origin of River Water Composition in Greece. In: N. Skoulikidis, E. Dimitriou, I. Karaouzas (eds.) The Rivers of Greece. Springer, Series: The Handbook of Environmental Chemistry, 97-128. https://doi.org/10.1007/978-3-662-55369-5.

Skoulikidis N., I. Karaouzas, Y. Amaxidis, M. Lazaridou (2021). Impact of EU Environmental Policy Implementation on the Quality and Status of Greek Rivers. Water 13, 1858. https://doi.org/10.3390/w13131858.

Skoulikidis N., A. Lampou, S. Laschou (2020). Unraveling aquatic quality controls of a nearly undisturbed Mediterranean Island (Samothraki, Greece). Water 12, 473; doi:10.3390/w12020473.

Skoulikidis N., L. Vardakas, Y. Amaxidis, P. Michalopoulos (2017). Biogeochemical processes controlling aquatic quality during drying and rewetting events in a Mediterranean non-perennial river reach. Science of the Total Environment 575, 378–389. doi: 10.1016/j.scitotenv.2016.10.015.

Skoulikidis N., A. Lampou, I. Karaouzas, K. Gritzalis, M. Lazaridou, S. Zogaris (2014). Stream ecological assessment on an Aegean island: Insights from an exploratory application on Samothraki (Greece). Fresenius Environ. Bull. 23, 1173–1182.

Skoulikidis N., Y. Amaxidis (2009). Origin and dynamics of dissolved and particulate nutrients in a minimally disturbed Mediterranean river with intermittent flow. Journal of Hydrology, 37: 218–229. https://doi.org/10.1016/j.jhydrol.2009.04.032.

Skoulikidis N., Y. Amaxidis, I. Bertahas, S. Laschou, K. Gritzalis (2006). Analysis of factors driving stream water composition and synthesis of management tools – A case study on small/medium Greek catchments. The Science of the Total Environment 362: 205-241. DOI: 10.1016/j.scitotenv.2005.05.016.

Smeti E., G. Tsirtsis, N. Skoulikidis (2023). Geology can drive the diversity-ecosystem functioning relationship in river benthic diatoms by selecting for species functional traits. Biology 12(1), 81. https://doi.org/10.3390/biology12010081.

Sun M., W. Wu, X. Ji, X. Wang, S. Qu (2018). Silicate weathering rate and its controlling factors: A study from small granitic watersheds in the Jiuhua Mountains. Chemical Geology 18981, https://doi.org/10.1016/j.chemgeo.2018.11.019.

Syrides G., K. Vouvalidis, K. Albanakis, P. Tsourlos, D. Matsas (2009). Palaeogeographical Evolution and Sea Level Changes during Holocene in the Prehistoric Settlement of Mikro

Vouni (Samothrace Island, Greece). Z. Geomorphol. Suppl. Issues, 53, 39–54. DOI: 10.1127/0372-8854/2009/0053S1-0039.

Taylor A.B., M.A. Velbel (1991). Geochemical mass balances and weathering rates in forested watersheds of the southern Blue Ridge II. Effects of botanical uptake terms. Geoderma 51, 29–50. https://doi.org/10.1016/0016-7061(91)90065-2.

Tripathi M., P.K. Yadav, B.R. Chahar, P. Dietrich (2021). A review on groundwater–surface water interaction highlighting the significance of streambed and aquifer properties on the exchanging flux. Environmental Earth Sciences 80, 604. https://doi.org/10.1007/s12665-021-09897-9.

Triska, F.J., A.P. Jackman, J.H. Duff, R.J. Avanzino (1994). Ammonium sorption to channel and riparian sediments: A transient storage pool for dissolved inorganic nitrogen. Biogeochemistry 26, 2, 67–83. http://www.jstor.org/stable/1469145.

Tsagkaraki M., C. Theodosi, M. Kanakidou, N. Mihalopoulos (2020) Atmospheric Deposition over the Aegean Sea and Its Impact on the Seawater Productivity. In: C. Anagnostou, A. Kostianoy, I. Mariolakos, P. Panayotidis M. Soilemezidou, G. Tsaltas (eds.). The Handbook of Environmental Chemistry. Springer, Berlin, Heidelberg. https://doi.org/10.1007/698_2020_679.

Tsikouras V. (1992). The ophiolites of Samothraki Island. PhD thesis Univ. of Patras, Greece.

Uemura, R., Matsui, Y., Yoshimura, K., Motoyama, H. and Yoshida, N., 2008. Evidence of deuterium excess in water vapor as an indicator of ocean surface conditions. Journal of Geophysical Research: Atmospheres, 113(D19). https://doi.org/10.1029/2008JD010209.

Van der Weijden C.H, F.A.L. Pacheco (2006). Hydrogeochemistry in the Vouga River basin (central Portugal): Pollution and chemical weathering. Applied Geochemistry 21, 4, 580-613. https://doi.org/10.1016/j.apgeochem. 2005.12.006.

Velbel M.A. (1992). Geochemical mass balances and weathering rates in forested watersheds of the southern Blue Ridge III. Cations budgets and the weathering rate of amphibole. Am. J. Sci. 292, 58–78. DOI 10.2475/ajs.285.10.904.

Velbel M.A. (1985). Hydrogeochemical constraints on mass balances in forested watersheds of the southern Appalachians. In: Drever, J.I. (Ed.), The Chemistry of Weathering. D. Reidel, Holland, pp. 231–247. DOI:10.1007/978-94-009-5333-8_14.

Velbel M.A, J.R. Price (2007). Solute geochemical mass-balances and mineral weathering rates in small watersheds: Methodology, recent advances, and future directions. Applied Geochemistry 22, 1682–1700. doi:10.1016/j.apgeochem.2007.03.029.

Vespasiano, G., Apollaro, C., De Rosa, R., Muto, F., La Rosa, S., Fiebig, J., Mulch, A. and Marini, L., 2015. The Small Spring Method (SSM) for the definition of stable isotope–elevation relationships in Northern Calabria (Southern Italy). Applied Geochemistry, 63, pp.333-346.

Viers J., G. Barroux, M. Pinelli P. Seyler, P. Oliva, B. Dupre,´ G.R. Boaventura (2005). The influence of the Amazonian floodplain ecosystems on the trace element dynamics of the Amazon River mainstem (Brazil). Sci.Total Environ. 339, 219–232. doi: 10.1016/j.scitotenv.2004.07.034.

Viers J., P. Oliva, J.-L. Dandurand, B. Dupre (2014). Chemical Weathering Rates, CO_2 Consumption, and Control Parameters Deduced from the Chemical Composition of Rivers. Treatise on Geochemistry, 7, 175-194. http://dx.doi.org/10.1016/B978-0-08-095975-7.00506-4.

Villalobos-Forbes M., G. Esquivel-Hernández, R. Sánchez-Murillo, R. Sánchez-Gutiérrez, I. Matiatos (2021). Stable isotopic characterization of nitrate wet deposition in the tropical urban atmosphere of Costa Rica. Environmental Science and Pollution Research, 28, pp.67577-67592. https://doi.org/10.1007/s11356-021-15327-x.

Vystavna Y., I. Matiatos, L.I. Wassenaar (2021a). Temperature and precipitation effects on the isotopic composition of global precipitation reveal long-term climate dynamics. Scientific reports 11(1), p.18503. https://doi.org/10.1038/s41598-021-98094-6.

Vystavna Y., A. Harjung, L.R. Monteiro, I. Matiatos, L.I. Wassenaar (2021b). Stable isotopes in global lakes integrate catchment and climatic controls on evaporation. Nature Communications, 12(1), p.7224. https://doi.org/10.1038/s41467-021-27569-x

Walling D.E., I.D.L. Foster (1975). Variations in the natural chemical concentration of river water during flood flows, and the lag effect: some further comments. Journal of Hydrology 26, 237–244. https://doi.org/10.1016/0022-1694(75)90005-0.

Wilson M.J. (2020). Dissolution and formation of quartz in soil environments: a review. Soil Science Annual, 71(2), 99–110, https://doi.org/10.37501/soilsa/122398.

Wang W., W. Xu, Jr. J.L. Collett, D. Liu, A. Zheng, A.J. Dore, X. Liu (2019). Chemical compositions of fog and precipitation at Sejila Mountain in the southeast Tibetan Plateau, China. Environmental Pollution 253, 560-568, https://doi.org/10.1016/j.envpol.2019.07.055.

Wu W., J. Yang, S. Xu, H. Yin (2008). Geochemistry of the headwaters of the Yangtze River, Tongtian He and Jinsha Jiang: Silicate weathering and CO_2 consumption. Applied Geochemistry 23 3712-3727. doi:10.1016/j.apgeochem.2008.09.005.

Authors contribution

Nikolaos Th. Skoulikidis: Conceptualization, Funding acquisition, Investigation, Supervision, Writing - Original Draft, Writing - Review & Editing, Visualization

Ioannis Matiatos: Software, Data Curation, Writing - Review & Editing

Panagiotis Michalopoulos: Software, Data Curation, Writing - Review & Editing

Evangelia Smeti: Formal analysis, Validation, Writing - Review & Editing

Cemil Özkan: Investigation, Writing - Original Draft

Konstantinos Akepsimaidis: Methodology, Writing - Review & Editing

Sofia Laschou: Validation, Data Curation, Writing - Review & Editing

Christine Stumpp: Resources, Supervision, Funding acquisition Writing - Review & Editing

Declaration of interests

☒The authors declare that they have no known competing financial interests or personal relationships that could have appeared to influence the work reported in this paper.

☐The authors declare the following financial interests/personal relationships which may be considered as potential competing interests:

Graphical abstract

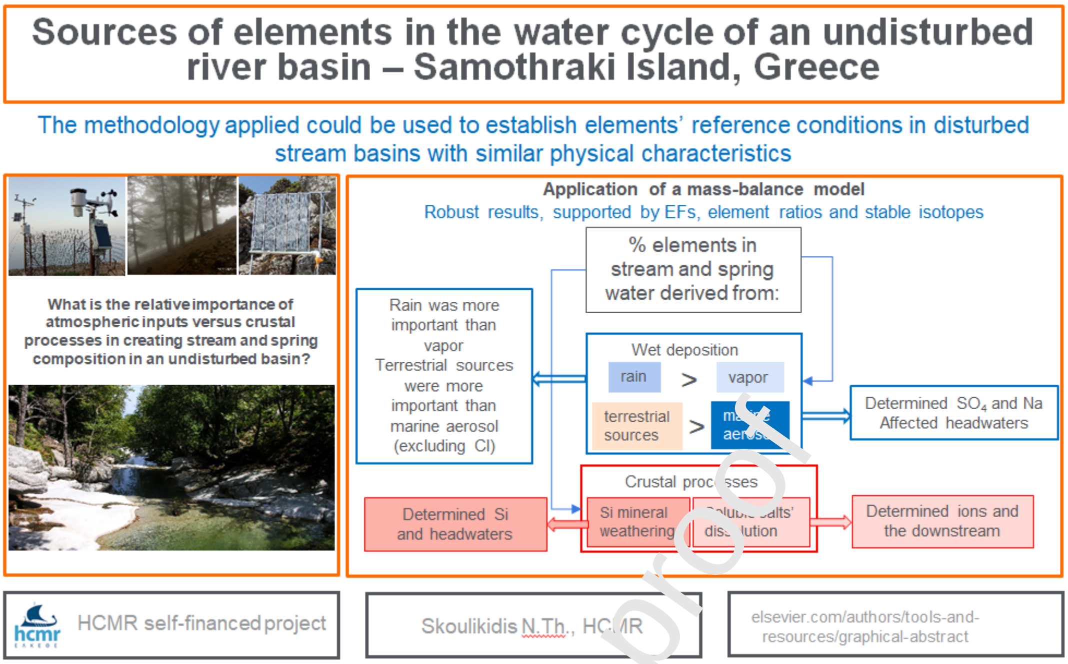

Highlights

- Vapor contributed to the water cycle of the basin
- Rain was more important element contributor than vapor
- Sulphate and sodium mainly derived from wet deposition
- Atmospheric inputs, silicate weathering and nitrification affected headwaters
- Salt dissolution and denitrification affected the downstream portion of the basin